An Indirect Torsional Vibration Receptance Measurement Method for Shaft Structures

Binglin Lv[a,b], Huajiang Ouyang[c], Wanyou Li[a], Zhijun Shuai[a] ,Gang Wang[a]
[a]College of Power and Energy Engineering, Harbin Engineering University, Harbin, 150001, P. R. China
[b]China Shipbuilding Power Engineering Institute Co. Ltd , Shanghai,120001 ,China
[c]School of Engineering, University of Liverpool, Liverpool, L69 3GH, UK

Corresponding author: Zhijun Shuai
College of Power and Energy Engineering
Harbin Engineering University
Harbin, 150001, P. R. China
Email address: shuaizhijun98@163.com

Email addresses: lvbinglin@aliyun.com(B. Lv), h.ouyang@liverpool.ac.uk (H. Ouyang), hrbeu_ripet_lwy@163.com (W. Li), shuaizhijun98@163.com（Z. Shuai）, wanggang.sjz@gmail.com(G. Wang)

Number of Pages: 47
Number of Figures: 24
Number of Tables: 0

ABSTRACT

In this paper, an indirect method for measuring torsional vibration of shaft structures is established. In conventional torsional vibration measurement, knowledge of two fundamental quantities is needed: a torque applied to the system and the angle of twist thus produced, which are both difficult to measure in experiment. In this indirect method, neither a deliberate torque excitation system nor an angular transducer is needed. Instead, a T-like beam structure is introduced and attached to one end of a shaft structure whereby the torques are produced by ordinary forces and only linear accelerometers at a few locations of the beam structure are used. Through the small finite element model of the T-like beam structure, the torsional receptance linking the torque to the angle of twist of the shafting systems is derived from the measured receptances of linear acceleration to the excitation force. This indirect theoretical-experimental combined method overcomes the difficulties and the associated poor accuracy in measuring receptances of torsional vibration of shaft structures, and hence is very useful. Numerical simulation of a test structure with noisy parameters and noisy simulated receptance data is made to validate the theoretical soundness of the method. Vibration tests are carried out on a laboratory shaft structure to demonstrate its accuracy and ease of use.

Keywords: Modal test; Receptance; Indirect Method; Torsional Vibration; Shaft; Uncertainty

Nomenclature

$\mathbf{B}_{ij}$	Dynamic stiffness of the shafting system
$\tilde{\mathbf{B}}_{ij}$	Dynamic stiffness of the T-like beam structure
$\mathbf{x}_0, \mathbf{x}_1, \mathbf{x}_2$	Vectors of displacements at connection point coordinates, other coordinates of the shafting system and other coordinates of the T-like beam structure, respectively
$\mathbf{f}_0, \mathbf{f}_2$	Forces externally applied at connection point coordinates and other coordinates of the T-like beam structure, respectively
w	Deflection in the *z* direction (see Figure 2)
θ_y	Rotational displacement about the *y* axis
θ_z	Rotational displacement about the *z* axis
f	Translational force applied in the *x* direction
T_y	Moment about the *y* axis
T_z	Torque about the *z* axis
$\hat{f}$	Internal translational force in the *x* direction
$\hat{T}_y$	Internal moment about the *y* axis
$\hat{T}_z$	Internal torque about the *z* axis
$\hat{f}_O$	Internal translational force in the *x* direction at point O
$\hat{T}_O$	Internal moment/torque about the *z* axis at point O
$\hat{\mathbf{f}}_0$	Internal force vector at connection point coordinates
$\tilde{\mathbf{H}}$	Receptance matrix of beam AOB
$\mathbf{H}$	Receptance matrix of parent structure SO
$\tilde{H}_{ij}$	Receptance of beam AOB between coordinates *i* and coordinate *j*
H_{ij}	Receptance of parent structure SO between coordinates *i* and coordinate *j*
H_{ij}^{measured}	Measured Receptance of assembled structure between coordinates *i* and coordinate *j*
$\hat{\mathbf{H}}$	Torsional Receptance matrix of beam OD
E	nominal Young's modulus
$\breve{E}$	Young's modulus with uncertainties
α	Percentage of uncertainty
RAN	A random value between 0 and 1
ρ	Density
l_{AB}	Length of beam AOB
h	height of beam AOB in the *z* direction
A_{me}	receptance without noise
$\breve{A}_{me}$	receptance with noise

1. Introduction

Shafts are common mechanical components that transmit mechanical power and withstand torques. In most cases, the torque a shaft bears would have a fluctuating component. When the frequency of this fluctuation is close to any torsional natural frequencies of the shaft, even a small torque can excite torsional resonance of the shaft and considerable damage may be caused to a machine such as fatigue failure, rapid bearing wear, gear hammering, fan belt slippage and often excessive noise problems [1-3]. Although many researchers have tried to measure frequency response function (FRF) data for rotational degrees-of-freedom (DOFs), only limited success has been made [4] and the accuracy of FRF of torsional vibration data is well known to be poor.

The problem of measuring torsional vibration can be tackled from two aspects: angular acceleration response measurement and torque excitation. Several techniques have been developed for torsional vibration tests based on measuring only the angular displacements of one or more points of a shafting without knowing accurately the value of torque excitation. Usually, angular velocity of shafting structures is measured by means of slotted discs, gears or magnetic pickups [5, 6]: one impulse is generated and detected once for every certain fraction of rotation of the shafting. Other similar devices such as grids or strips on the shaft as the target or rotary incremental encoders being installed at the free end of a shafting are also utilized [7]. For such a kind of measurement, a sufficient number of uniformly spaced teeth are of vital importance to maximize signal-to-noise ratios from the pickups. Optical methods involving lasers and the Doppler principle for angular vibration measurement [2, 8] are gaining acceptance as the standard means of measuring torsional vibration due to their merits over previously mentioned methods.

Although several techniques have been proposed for measuring rotational FRFs, few are proposed or applied for measuring torsional FRFs. A pair of matched conventional linear accelerometers placed a short distance apart on a structure to be measured, or on a fixture attached to a structure are often utilized for measuring rotational FRFs [4]: the translational and angular displacements of a structure at the centre point between these two accelerometers can then be deduced. Duarte and Ewins [9] gave a comprehensive table showing several studies done for measuring rotational degrees of freedom and proposed one improved close-accelerometers method by considering residual compensation. When it turns to torque measurement for torsional vibration of shafting, strain-gauge rosettes are usually utilized. For transferring signals from strain-gauge rosettes, a slip ring or telemetry is commonly required [5]. For rotating structures, hydraulic torsional exciter and electromagnetic exciter systems are always introduced to apply a dynamic torque. Sihler [10] presented a novel exciter for applying a dynamic torsional force to a rotating structure which can be easily applied in cases where a three-phase electrical machine is contained in a shaft assembly. Kim et al. [11] investigated the possibility of non-contact modal tests for torsional vibration of cylindrical bodies like pipes by an electromagnetic exciter.

However, in the literature about torsional vibration tests, studies of methods for measuring torsional receptance are rarely reported, even though this information is very useful in practice and actual measurement is known to be error-prone. This lack of information suggests that development of an effective method for measuring torsional receptance is necessary. In engineering design stage, theoretical models are always used for evaluating the torsional vibration characteristics of a shafting system. For a shafting system, some parameters (for examples, inertias of electrical machines and dynamic stiffness of couplings) cannot be obtained easily or even obtained at all, especially when these parts are assembled. Consequently, the

theoretical torsional vibration model of a shafting is very likely to have a poor accuracy. Torsional vibration measurement is then needed to validate or update the model. Measured vibration data is vitally important if a finite element model needs to be updated successfully [12]. Instead of updating a theoretical model, experimental data can also be used to construct a modal model of a structure or even used for fault identification of rotor systems [13-17]. Ricci et al. [18] updated their torsional vibration model of an industrial steam turbo generator based on only measured torsional natural frequencies. Pennacchi et al. [19, 20] used a modal representation of the supporting structure for a rotating machine to increase the accuracy of fault identification. When restricted by the measurement technology, identification of parameters would be very difficult. Prediction of dynamic behaviour of a shafting based on such a theoretical model is not very accurate, let alone structural optimisation or structural control for performance improvement based on such a model. For example, it is impossible to achieve the objective of good vibration reduction for some industrial problems [21] in these situations.

Structural modifications are an effective method for improving a structure's dynamic behaviour. These rely on accurate measurement of modal data or FRF data of the structure concerned. Structural modification methods using measured receptance or FRFs were studied for determining FRFs of the modified structure [22] or assigning vibration nodes [23], natural frequencies and zeroes [24] or even eigenstructure [25] of the modified structure. For such receptance-based methods, finite element models of structures are no longer needed and thus the difficulties in modelling mentioned previously no longer occur. These methods require accurate measured FRFs. It should be pointed out that these receptance-based methods have not been applied to rotating machineries, perhaps partly because of the difficulties in accurate measurement of torsional FRFs.

In torsional vibration measurement and some other real engineering situations, ‘forces’ (especially torques) or displacements (especially rotation) cannot be measured directly in an accurate manner. However, to fully understand the vibration characteristics of structure, knowledge of the forces applied or displacements that are difficult to measure directly is always desirable. To overcome such difficulties, several indirect methods have been proposed. Dobson and Eider [26] reviewed the indirect calculation of excitation forces from measured structural response data before 1990. Pennacchi [27, 28] proposed the M-estimators to excitation identification in mechanical systems. Li et al. [29] presented a novel load identification method based on wavelet multi-resolution analysis using the Impulse Response Function of the system. Avitabile and O’Callahan [30] estimated the unmeasured rotations from a finite element model expanded from the measured translational displacements. Yap and Gibbs [31, 32] indirectly measured the force and moment induced power flow of a built-up machine by a reciprocal method but did not get as far as determination of rotational receptances.

Furthermore, some researchers have extended such indirect methods of measuring point moment mobility of structures. Sanderson and Fredo [33, 34] proposed two two-exciter methods for measuring moment mobility with a T-like block and an I-like block, by which the moment applied to a structure can be achieved indirectly. Su and Gibbs [35] discussed theoretically the discrepancy between the measured and true moment mobilities when an unbalanced force was present as a result of using a pair of matched shakers. Silva et al. [36] modified the Mass Uncoupling Method (MUM) for indirect estimation of rotational FRFs by means of an added T-block (with the effect of mass and inertia of the T-block removed). Different from the afore-mentioned methods, Dong and McConnel [37] assumed the supplemental fixture of a test structure as elastic instead of rigid and then modelled it using the finite element method to

estimate the rotational receptance of the test structure. In this method, rotational accelerometers or strain gauges which could output high quality rotational acceleration signals were required. Mottershead et al. [38-40] proposed one indirect method using an elastic T-block for estimation of rotational receptances. However, none of these papers are about torsional vibration measurement of shafting structures. Nevertheless, these works on measuring rotations in bending vibration inspired the present work on torsional vibration.

In this paper, a new method for measuring the torsional receptance at one end of a shafting structure is presented by connecting a T-like beam structure to the shafting. The relationship between the translational receptances of the combined system and the torsional receptance of the original shafting is derived. Then the torsional receptance can be estimated with conventional linear acceleration transducers and an impact hammer while neither angular acceleration measurements nor torque measurements are required. Theoretical development of the proposed procedure are presented in section 2. In section 3, the factors affecting estimation accuracy of the torsional receptance are also analysed based on a finite element model with simulated noise included. Finally, in section 4, the method is applied to one real laboratory structure and the estimated torsional receptances are compared under different measurement setups.

2. Theoretical Development

2.1 Theoretical Development

As shown in Fig. 1, a shafting system is attached with a T-like beam structure AOBD where D is the connection point between the shafting and the attached T-like beam structure. The aim is to obtain the torsional receptance at connection point D of the shafting system (without the T-like beam structure AOBD). Firstly, dynamic characteristics of the T-like beam structure AOBD must be understood.

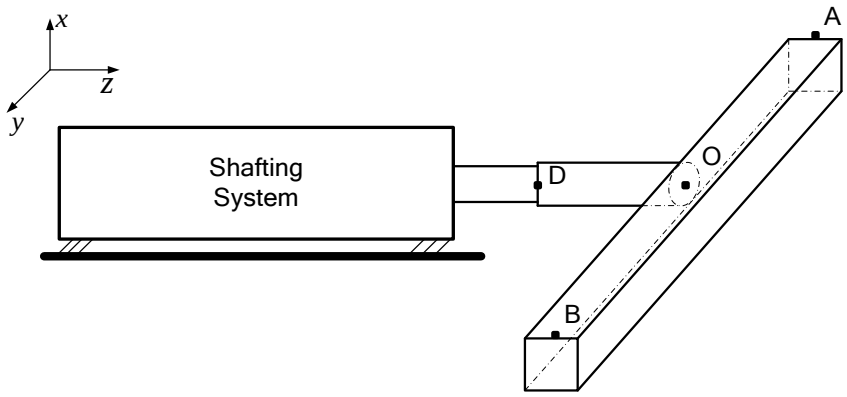

Fig. 1 The assembled structure of the shafting system and the T-like beam structure

As can be seen from Fig. 1, the torsional vibration of beam OD about the *z* axis is coupled with the bending vibration of beam AOB in the *x*-*y* plane. In this way, when beam AOB is excited at points A and B in the *x* direction, the bending vibration of beam AOB and the torsional vibration of beam OD are related.

Similarly to [38], the equation of motion of the assembled structure (the original shafting system and the T-like beam structure AOBD together) in the frequency domain can be written as

$$\begin{bmatrix} \mathbf{B}_{11}(\omega) & \mathbf{B}_{10}(\omega) & \mathbf{0} \\ \mathbf{B}_{01}(\omega) & \mathbf{B}_{00}(\omega) & \mathbf{0} \\ \mathbf{0} & \mathbf{0} & \mathbf{0} \end{bmatrix} \begin{pmatrix} \mathbf{x}_1 \\ \mathbf{x}_0 \\ \mathbf{x}_2 \end{pmatrix} = \begin{pmatrix} \mathbf{0} \\ \mathbf{f}_0 \\ \mathbf{f}_2 \end{pmatrix} - \begin{bmatrix} \mathbf{0} & \mathbf{0} & \mathbf{0} \\ \mathbf{0} & \tilde{\mathbf{B}}_{00}(\omega) & \tilde{\mathbf{B}}_{02}(\omega) \\ \mathbf{0} & \tilde{\mathbf{B}}_{20}(\omega) & \tilde{\mathbf{B}}_{22}(\omega) \end{bmatrix} \begin{pmatrix} \mathbf{x}_1 \\ \mathbf{x}_0 \\ \mathbf{x}_2 \end{pmatrix} \tag{1}$$

where matrices $\mathbf{B}_{ij}$ on the left represent the dynamic stiffness of the shafting system and matrices $\tilde{\mathbf{B}}_{ij}$ on the right represent the dynamic stiffness of T-like beam structure AOBD. Subscripts 0, 1 and 2 denote the connection point coordinates, the other coordinates of the shafting system and the other coordinates of the T-like beam structure, respectively, and $\mathbf{x}_0$, $\mathbf{x}_1$ and $\mathbf{x}_2$ are the vectors of displacements at coordinates 0, 1 and 2; while the force vectors $\mathbf{f}_0$ and $\mathbf{f}_2$ are for the internal forces coordinates 0 and the forces externally applied at coordinates 2, respectively.

2.2 Proposed Procedure

One T-like beam structure AOBD as show in Fig. 2 is attached to the shafting system, where w_D, θ_{yD} and θ_{zD} are the flexural displacement in the *x* direction, rotational displacements about the *y* axis and *z* axis of point D, respectively. $\mathbf{f}_2$, T_{yD}, T_{zD} and f_D are the external forces applied at the T-like beam structure, the moment applied about the *y* axis and the torque applied about the *z* axis at point D, and the translational force applied in the *x* direction, respectively.

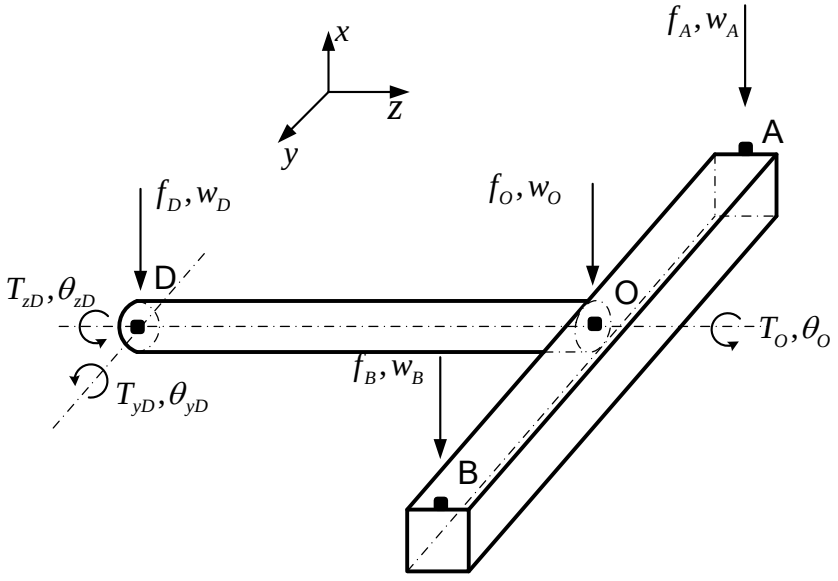

Fig. 2 T-like beam structure

Taking the T-like beam structure as a free body, the total influence of the shafting on the attached structure can be represented by an internal force, an internal moment and an internal torque, denoted respectively by $\hat{f}_D$, $\hat{T}_{yD}$ and $\hat{T}_{zD}$ when the assembled structure is excited at points A, O and B in the *x* direction. The equation of motion of the T-like beam structure can thus be expressed as,

$$\begin{bmatrix} \tilde{\mathbf{B}}_{w_D w_D}(\omega) & \tilde{\mathbf{B}}_{w_D \theta_{yD}}(\omega) & \tilde{\mathbf{B}}_{w_D \theta_{zD}}(\omega) & \tilde{\mathbf{B}}_{w_D 2}(\omega) \\ \tilde{\mathbf{B}}_{\theta_{y0} w_D}(\omega) & \tilde{\mathbf{B}}_{\theta_{yD} \theta_{yD}}(\omega) & \tilde{\mathbf{B}}_{\theta_{yD} \theta_{zD}}(\omega) & \tilde{\mathbf{B}}_{\theta_{yD} 2}(\omega) \\ \tilde{\mathbf{B}}_{\theta_{zD} w_D}(\omega) & \tilde{\mathbf{B}}_{\theta_{zD} \theta_{yD}}(\omega) & \tilde{\mathbf{B}}_{\theta_{zD} \theta_{zD}}(\omega) & \tilde{\mathbf{B}}_{\theta_{zD} 2}(\omega) \\ \tilde{\mathbf{B}}_{2 w_D}(\omega) & \tilde{\mathbf{B}}_{2 \theta_{yD}}(\omega) & \tilde{\mathbf{B}}_{2 \theta_{zD}}(\omega) & \tilde{\mathbf{B}}_{22}(\omega) \end{bmatrix} \begin{pmatrix} w_D(\omega) \\ \theta_{yD}(\omega) \\ \theta_{zD}(\omega) \\ \mathbf{x}_2 \end{pmatrix} = \begin{pmatrix} \hat{f}_D(\omega) \\ \hat{T}_{yD}(\omega) \\ \hat{T}_{zD}(\omega) \\ \mathbf{f}_2 \end{pmatrix} \tag{2}$$

In this equation, $\mathbf{f}_2$, $\mathbf{x}_2$ and w_D can be obtained from a modal experiment, while all the other unknown terms $\hat{f}_D$, $\hat{T}_{yD}$, $\hat{T}_{zD}$, θ_{yD} and θ_{zD} representing the internal 'forces', and rotational and angular displacements at connection point D need to be determined. The purpose of this paper is to estimate the torsional receptance, so only $\hat{T}_{zD}$ and θ_{zD} are needed here. If Eq. (2) is utilized, both torsional and bending parts of beams AOB and OD of the T-block should be modelled. There are three redundant unknowns in Eq. (2) which may affect the accuracy of the estimated torsional receptance when the measured data contains noise, and hence they should be removed.

In order to avoid building a complex FE model and minimise the number of unknowns to estimate, one indirect method is established here to improve the accuracy of torsional receptance estimation. Instead of estimating the torsional receptance from Eq. (2) directly, the previously mentioned difficulties can be overcome by dividing the estimation process into two steps. The first step is to estimate the torsional receptance at point O of the shafting system with beam OD (for convenience, in the following part of this paper, the shafting system combined with beam OD is called structure SO): in this step, only the bending of beam AOB is included. The second step is to estimate the torsional receptance of the shafting system at point D from the torsional receptance of structure SO: in this step, the bending of beam OD does not need to be considered and only its torsion is included. These two steps are described in detail as follows. Of course, in case when one single beam AOB can be connected to a shafting system without any other accessorial components, the second step is then no longer needed. In this paper, although

theoretical derivation is given for both steps, step one is used, since the laboratory structure used to validate the present method allows direction connection of beam AOB to the shafting.

2.3 Frequency Response Function Estimation

2.3.1 Step 1: Estimation of the torsional receptance at point O

For the first step, when considering point O instead of point D, the shafting system with beam OD is now considered the original structure or parent structure as a whole. For point O, the angular displacement about the *z* axis of structure SO is equal to the rotation of the bending vibration of beam AOB in the *x*-*y* plane. Two different procedures are presented with different measurement positions used for step 1 here.

2.3.1.1 Procedure 1: Measuring Point A and Point O

The procedure on how to estimate the torsional receptance at point O of structure SO from the FRFs obtained when beam AOB is attached is derived below using measured data at centre point O and one end point A (or point B).

Instead of Eq. (1), the dynamics of both sub-structure SO and beam AOB can also be described separately using the internal 'forces' $\hat{f}_O$ and $\hat{T}_O$ and displacements w_O and θ_O at the connection point. As the receptance matrix can be obtained more easily (and more accurately as the reduction of stiffness and mass matrices is no longer needed), here the receptance matrix equation of beam AOB is used. The equation of motion of beam AOB can then be expressed in an accurate receptance form as

$$\begin{bmatrix} \tilde{\mathbf{H}}_{00}(\omega) & \tilde{\mathbf{H}}_{02}(\omega) \\ \tilde{\mathbf{H}}_{20}(\omega) & \tilde{\mathbf{H}}_{22}(\omega) \end{bmatrix} \begin{pmatrix} \hat{\mathbf{f}}_0 \\ \mathbf{f}_2 \end{pmatrix} = \begin{pmatrix} \mathbf{x}_0 \\ \mathbf{x}_2 \end{pmatrix} \tag{3}$$

where matrices $\tilde{\mathbf{H}}_{ij}$ on the left represent the receptance of beam AOB.

As in a real experimental test, not all displacements of a structure can be measured, such as the rotational terms. Hence, these unmeasured degrees of freedom are usually eliminated from the above equation.

Since for the parent structure the internal 'forces' act at the connection point in the opposite direction in relation to the attached beam structure, the equation of motion of the parent structure SO can be expressed as

$$\mathbf{H}_{00}(\omega)\left(-\hat{\mathbf{f}}_0\right)=\mathbf{x}_0 \tag{4}$$

where $\hat{\mathbf{f}}_0=\left\{\hat{f}_O(\omega) \quad \hat{T}_O(\omega)\right\}^{\mathrm{T}}$ and $\mathbf{x}_0=\left\{w_O(\omega) \quad \theta_O(\omega)\right\}^{\mathrm{T}}$. Only connection point O is concerned in Eq. (4).

In the case when point A is excited, Eq. (3) can be rewritten as

$$\begin{pmatrix} w_O(\omega) \\ \theta_O(\omega) \\ w_A(\omega) \end{pmatrix}=\begin{bmatrix} \tilde{H}_{w_Ow_O}(\omega) & \tilde{H}_{w_O\theta_O}(\omega) & \tilde{H}_{w_Ow_A}(\omega) \\ \tilde{H}_{\theta_Ow_O}(\omega) & \tilde{H}_{\theta_O\theta_O}(\omega) & \tilde{H}_{\theta_Ow_A}(\omega) \\ \tilde{H}_{w_Aw_O}(\omega) & \tilde{H}_{w_A\theta_O}(\omega) & \tilde{H}_{w_Aw_A}(\omega) \end{bmatrix}\begin{pmatrix} \hat{f}_O(\omega) \\ \hat{T}_O(\omega) \\ f_A(\omega) \end{pmatrix} \tag{5}$$

In Eq. (5), f_A, w_A and w_O are obtained from a test, and the receptance matrix elements of (denoted by $\tilde{H}_{ij}$) beam AOB can be calculated from its finite element model. The unknowns are $\hat{f}_O$, $\hat{T}_O$ and θ_O, which can then be calculated from Eq. (5). By moving all the unknowns to the left-hand side, Eq. (5) becomes,

$$\begin{bmatrix} \tilde{H}_{w_Ow_O}(\omega) & \tilde{H}_{w_O\theta_O}(\omega) & 0 \\ \tilde{H}_{\theta_Ow_O}(\omega) & \tilde{H}_{\theta_O\theta_O}(\omega) & -1 \\ \tilde{H}_{w_Aw_O}(\omega) & \tilde{H}_{w_A\theta_O}(\omega) & 0 \end{bmatrix}\begin{pmatrix} \hat{f}_O(\omega) \\ \hat{T}_O(\omega) \\ \theta_O(\omega) \end{pmatrix}=\begin{pmatrix} w_O(\omega)-\tilde{H}_{w_Ow_A}(\omega)f_A \\ -\tilde{H}_{\theta_Ow_A}(\omega)f_A \\ w_A(\omega)-\tilde{H}_{w_A}(\omega)f_A \end{pmatrix} \tag{6}$$

with which, all the unknowns including two internal 'forces' $\hat{f}_O$ and $\hat{T}_O$ and one rotation θ_O can be obtained.

For beam AOB, w_O and θ_O are coupled together, which means that cross receptances $H_{w_O\theta_O}(\omega)$ and $H_{\theta_O w_O}(\omega)$ are not equal to zero. However, for linear rotor dynamics of simple straight shafting (excluding general cases such as crank shafting, shafting with gears, unbalanced and cracked rotors, etc.), the assumption that the torsional vibration (θ_O) and bending vibration (w_O) are uncoupled with each other is valid [3], which means for structure SO in these special cases,

$$H_{w_O\theta_O}(\omega) = H_{\theta_O w_O}(\omega) = 0 \tag{7}$$

With Eq. (7) and Eq. (4), the torsional receptance can then be calculated as

$$H_{\theta_O\theta_O}(\omega) = -\frac{\theta_O(\omega)}{\hat{T}_O(\omega)} \tag{8}$$

By dividing both sides by f_A, Eq. (6) can be rewritten as

$$\begin{bmatrix} \tilde{H}_{w_O w_O}(\omega) & \tilde{H}_{w_O\theta_O}(\omega) & 0 \\ \tilde{H}_{\theta_O w_O}(\omega) & \tilde{H}_{\theta_O\theta_O}(\omega) & -1 \\ \tilde{H}_{w_A w_O}(\omega) & \tilde{H}_{w_A\theta_O}(\omega) & 0 \end{bmatrix} \begin{pmatrix} \frac{\hat{f}_O}{f_A} \\ \frac{\hat{T}_O}{f_A} \\ \frac{\theta_O}{f_A} \end{pmatrix} = \begin{pmatrix} -\tilde{H}_{w_O w_A}(\omega) \\ -\tilde{H}_{\theta_O w_A}(\omega) \\ -\tilde{H}_{w_A w_A}(\omega) \end{pmatrix} + \begin{pmatrix} H^{\text{measured}}_{w_O w_A}(\omega) \\ 0 \\ H^{\text{measured}}_{w_A w_A}(\omega) \end{pmatrix} \tag{9}$$

where $H^{\text{measured}}_{w_O w_A}(\omega) = w_O / f_A$ and $H^{\text{measured}}_{w_A w_A}(\omega) = w_A / f_A$ are respectively the related cross receptance between A(B) and O, and the point receptance at point A(B). The internal torque $\hat{T}_O$ and torsional angle θ_O about axis *z* can now be calculated directly by solving the following equations:

$$\hat{T}_O = -\frac{\tilde{H}_{w_A w_O}\left(H^{\text{measured}}_{w_O w_A} - \tilde{H}_{w_O w_A}\right)}{\tilde{H}_{w_O w_O}\tilde{H}_{w_A\theta_O} - \tilde{H}_{w_A w_O}\tilde{H}_{w_O\theta_O}} + \frac{\tilde{H}_{w_O w_O}\left(H^{\text{measured}}_{w_A w_A} - \tilde{H}_{w_A w_A}\right)}{\tilde{H}_{w_O w_O}\tilde{H}_{w_A\theta_O} - \tilde{H}_{w_A w_O}\tilde{H}_{w_O\theta_O}} \tag{10}$$

$$\theta_O = \frac{\left(\tilde{H}_{w_O\theta_O}\tilde{H}_{w_A\theta_O} - \tilde{H}_{\theta_O\theta_O}\tilde{H}_{w_Aw_O}\right)\left(h^{\text{measured}}_{w_Ow_A} - \tilde{H}_{w_Ow_A}\right)}{\tilde{H}_{w_Ow_O}\tilde{H}_{w_A\theta_O} - \tilde{H}_{w_Aw_O}\tilde{H}_{w_O\theta_O}} + \tilde{H}_{\theta_Ow_A} + \frac{\left(\tilde{H}_{w_Ow_O}\tilde{H}_{\theta_O\theta_O} - \tilde{H}^2_{w_O\theta_O}\right)\left(h^{\text{measured}}_{w_Aw_A} - \tilde{H}_{w_Aw_A}\right)}{\tilde{H}_{w_Ow_O}\tilde{H}_{w_A\theta_O} - \tilde{H}_{w_Aw_O}\tilde{H}_{w_O\theta_O}} \tag{11}$$

2.3.1.2 Procedure 2: Measuring Point A and Point B

In procedure 1, as Eq. (7) is used, its applicability is actually limited. For this reason, procedure 2 is proposed here. Instead of measured data at point O, measured data at point B is included. Eq. (3) can then be rewritten as,

$$\begin{pmatrix} w_O \\ \theta_O \\ w_A \\ w_B \end{pmatrix} = \begin{bmatrix} \tilde{H}_{w_Ow_O}(\omega) & \tilde{H}_{w_O\theta_O}(\omega) & \tilde{H}_{w_Ow_A}(\omega) & \tilde{H}_{w_Ow_B}(\omega) \\ \tilde{H}_{\theta_Ow_O}(\omega) & \tilde{H}_{\theta_O\theta_O}(\omega) & \tilde{H}_{\theta_Ow_A}(\omega) & \tilde{H}_{\theta_Ow_B}(\omega) \\ \tilde{H}_{w_Aw_O}(\omega) & \tilde{H}_{w_A\theta_O}(\omega) & \tilde{H}_{w_Aw_A}(\omega) & \tilde{H}_{w_Aw_B}(\omega) \\ \tilde{H}_{w_Bw_O}(\omega) & \tilde{H}_{w_B\theta_O}(\omega) & \tilde{H}_{w_Bw_A}(\omega) & \tilde{H}_{w_Bw_B}(\omega) \end{bmatrix} \begin{pmatrix} \hat{f}_O \\ \hat{T}_O \\ f_A \\ f_B \end{pmatrix} \tag{12}$$

From Eq. (12), the internal ‘forces’ and responses can be expressed as,

$$\begin{pmatrix} \hat{f}_O \\ \hat{T}_O \end{pmatrix} = \left(\begin{bmatrix} \tilde{H}_{w_Aw_O}(\omega) & \tilde{H}_{w_A\theta_O}(\omega) \\ \tilde{H}_{w_Bw_O}(\omega) & \tilde{H}_{w_B\theta_O}(\omega) \end{bmatrix} \right)^{-1} \left(\begin{pmatrix} w_A \\ w_B \end{pmatrix} - \begin{bmatrix} \tilde{H}_{w_Aw_A}(\omega) & \tilde{H}_{w_Aw_B}(\omega) \\ \tilde{H}_{w_Bw_A}(\omega) & \tilde{H}_{w_Bw_B}(\omega) \end{bmatrix} \begin{pmatrix} f_A \\ f_B \end{pmatrix} \right) \tag{13}$$

and

$$\begin{pmatrix} w_O \\ \theta_O \end{pmatrix} = \begin{bmatrix} \tilde{H}_{w_Ow_O}(\omega) & \tilde{H}_{w_O\theta_O}(\omega) \\ \tilde{H}_{\theta_Ow_O}(\omega) & \tilde{H}_{\theta_O\theta_O}(\omega) \end{bmatrix} \begin{pmatrix} \hat{f}_O \\ \hat{T}_O \end{pmatrix} + \begin{bmatrix} \tilde{H}_{w_Ow_A}(\omega) & \tilde{H}_{\theta_Ow_A}(\omega) \\ \tilde{H}_{w_Ow_B}(\omega) & \tilde{H}_{\theta_Ow_B}(\omega) \end{bmatrix} \begin{pmatrix} f_A \\ f_B \end{pmatrix} \tag{14}$$

What should be noticed here is that there exist two load conditions: point A is excited and no force is applied to point B; and point B is excited and no force is applied to point A (referred to as single load cases). Even with the single load case, when internal torque $\hat{T}_O$ and angle θ_O are estimated using Eq. (13) and Eq. (14), the torsional receptance can also be obtained using Eq. (8). In order to improve the estimation results, both measurement data with two different load

conditions is used: by combining all the estimated internal forces and estimated displacements at point O, the equation of motion of the shafting can then be rewritten as

$$\mathbf{H}_{00}(\omega)\left(\begin{bmatrix}\mathbf{R}(\omega) & \mathbf{S}(\omega)\end{bmatrix}\begin{bmatrix}\mathbf{X}_2(\omega)\\ \mathbf{I}_{2\times 2}\end{bmatrix}\right)=\begin{bmatrix}\mathbf{T}(\omega) & \mathbf{U}(\omega)\end{bmatrix}\begin{bmatrix}\mathbf{X}_2(\omega)\\ \mathbf{I}_{2\times 2}\end{bmatrix} \tag{15}$$

where

$$\mathbf{R}(\omega)=\left(\begin{bmatrix}\tilde{H}_{w_A w_O}(\omega) & \tilde{H}_{w_A \theta_O}(\omega)\\ \tilde{H}_{w_B w_O}(\omega) & \tilde{H}_{w_B \theta_O}(\omega)\end{bmatrix}\right)^{-1} \tag{16-a}$$

$$\mathbf{S}(\omega)=-\mathbf{R}(\omega)\begin{bmatrix}\tilde{H}_{w_A w_A}(\omega) & \tilde{H}_{w_A w_B}(\omega)\\ \tilde{H}_{w_B w_A}(\omega) & \tilde{H}_{w_B w_B}(\omega)\end{bmatrix} \tag{16-b}$$

$$\mathbf{T}(\omega)=\begin{bmatrix}\tilde{H}_{w_O w_O}(\omega) & \tilde{H}_{w_O \theta_O}(\omega)\\ \tilde{H}_{\theta_O w_O}(\omega) & \tilde{H}_{\theta_O \theta_O}(\omega)\end{bmatrix}\mathbf{R}(\omega) \tag{16-c}$$

$$\mathbf{U}(\omega)=\begin{bmatrix}\tilde{H}_{w_O w_O}(\omega) & \tilde{H}_{w_O \theta_O}(\omega)\\ \tilde{H}_{\theta_O w_O}(\omega) & \tilde{H}_{\theta_O \theta_O}(\omega)\end{bmatrix}\mathbf{S}(\omega)+\begin{bmatrix}\tilde{H}_{w_O w_A}(\omega) & \tilde{H}_{\theta_O w_A}(\omega)\\ \tilde{H}_{w_O w_B}(\omega) & \tilde{H}_{\theta_O w_B}(\omega)\end{bmatrix} \tag{16-d}$$

and

$$\mathbf{X}_2(\omega)=\begin{bmatrix}H_{w_A w_A}^{\text{measured}}(\omega) & H_{w_A w_B}^{\text{measured}}(\omega)\\ H_{w_B w_A}^{\text{measured}}(\omega) & H_{w_B w_B}^{\text{measured}}(\omega)\end{bmatrix} \tag{16-e}$$

Post-multiplying both sides of Eq. (15) like in [38] by

$$\begin{bmatrix}\mathbf{X}_2^{*\mathrm{T}}(\omega) & \mathbf{I}_{2\times 2}\end{bmatrix}\begin{bmatrix}\mathbf{R}^{*\mathrm{T}}(\omega)\\ \mathbf{S}^{*\mathrm{T}}(\omega)\end{bmatrix} \tag{17}$$

and taking *n* averages for each of the two separate load cases leads to H_1 estimator expression:

$$\mathbf{H}_{00}(\omega)=\mathbf{B}(\omega)\mathbf{A}^{-1}(\omega) \tag{18}$$

$$\mathbf{A}(\omega)=\begin{bmatrix}\mathbf{R}(\omega) & \mathbf{S}(\omega)\end{bmatrix}\begin{bmatrix}\mathbf{G}_{x_2 x_2} & \mathbf{G}_{x_2 f_2}\\ \mathbf{G}_{f_2 x_2} & \mathbf{G}_{f_2 f_2}\end{bmatrix}\begin{bmatrix}\mathbf{R}^{*\mathrm{T}}(\omega)\\ \mathbf{S}^{*\mathrm{T}}(\omega)\end{bmatrix} \tag{19}$$

$$\mathbf{B}(\omega)=\begin{bmatrix}\mathbf{T}(\omega) & \mathbf{U}(\omega)\end{bmatrix}\begin{bmatrix}\mathbf{G}_{x_2x_2} & \mathbf{G}_{x_2f_2}\\ \mathbf{G}_{f_2x_2} & \mathbf{G}_{f_2f_2}\end{bmatrix}\begin{bmatrix}\mathbf{R}^{*\mathrm{T}}(\omega)\\ \mathbf{S}^{*\mathrm{T}}(\omega)\end{bmatrix} \tag{20}$$

Alternatively, post-multiply both sides of Eq. (15) by

$$\begin{bmatrix}\mathbf{X}_2^{*\mathrm{T}}(\omega) & \mathbf{I}_{2\times 2}\end{bmatrix}\begin{bmatrix}\mathbf{T}^{*\mathrm{T}}(\omega)\\ \mathbf{U}^{*\mathrm{T}}(\omega)\end{bmatrix} \tag{21}$$

and taking *n* averages for each of the two separate load cases leads to H_2 estimator expression:

$$\mathbf{H}_{00}(\omega)=\mathbf{D}(\omega)\mathbf{C}^{-1}(\omega) \tag{22}$$

$$\mathbf{C}(\omega)=\begin{bmatrix}\mathbf{R}(\omega) & \mathbf{S}(\omega)\end{bmatrix}\begin{bmatrix}\mathbf{G}_{x_2x_2} & \mathbf{G}_{x_2f_2}\\ \mathbf{G}_{f_2x_2} & \mathbf{G}_{f_2f_2}\end{bmatrix}\begin{bmatrix}\mathbf{T}^{*\mathrm{T}}(\omega)\\ \mathbf{U}^{*\mathrm{T}}(\omega)\end{bmatrix} \tag{23}$$

$$\mathbf{D}(\omega)=\begin{bmatrix}\mathbf{T}(\omega) & \mathbf{U}(\omega)\end{bmatrix}\begin{bmatrix}\mathbf{G}_{x_2x_2} & \mathbf{G}_{x_2f_2}\\ \mathbf{G}_{f_2x_2} & \mathbf{G}_{f_2f_2}\end{bmatrix}\begin{bmatrix}\mathbf{T}^{*\mathrm{T}}(\omega)\\ \mathbf{U}^{*\mathrm{T}}(\omega)\end{bmatrix} \tag{24}$$

The submatrices, typically $\mathbf{G}_{x_2f_2}(\omega)$, contain power spectral densities. For example,

$$\mathbf{G}_{x_2f_2}(\omega)=\sum_1^2\frac{1}{n}\sum_{i=1}^{n}\begin{bmatrix}x_A^i f_A^i & x_A^i f_B^i\\ x_B^i f_A^i & x_B^i f_B^i\end{bmatrix} \tag{25}$$

2.3.2 Step 2: Estimation of the torsional receptance at point D

However, in real applications, often the foregoing derivations may not be good enough for estimating torsional receptance: what is needed is the torsional receptance at point D instead of point O in most cases as more often another component (likely to be a short beam) will be attached to one end of the shafting in order that these two structures can be assembled. Therefore, a second step to estimate the torsional receptance of the shafting system at point D from the torsional receptance of structure SO at point O is derived. Taking beam OD as a free body, its equation of motion can be written as,

$$\begin{bmatrix} \hat{H}_{\theta_O\theta_O}(\omega) & \hat{H}_{\theta_O\theta_D}(\omega) \\ \hat{H}_{\theta_D\theta_O}(\omega) & \hat{H}_{\theta_D\theta_D}(\omega) \end{bmatrix} \begin{Bmatrix} T_{\theta_O} \\ T_{\theta_D} \end{Bmatrix} = \begin{Bmatrix} \theta_O \\ \theta_D \end{Bmatrix} \tag{26}$$

Receptance matrix $\hat{\mathbf{H}}$ is calculated using the torsional vibration finite element model of beam OD. By dividing θ_D on both sides of Eq. (26) and moving all the unknowns from the right to the left, the equation becomes

$$\begin{bmatrix} \hat{H}_{\theta_O\theta_O}(\omega) - H_{\theta_O\theta_O}(\omega) & \hat{H}_{\theta_O\theta_D}(\omega) \\ \hat{H}_{\theta_D\theta_O}(\omega) & \hat{H}_{\theta_D\theta_D}(\omega) \end{bmatrix} \begin{Bmatrix} \dfrac{T_{\theta_O}}{\theta_D} \\ -\dfrac{1}{H_{\theta_D\theta_D}(\omega)} \end{Bmatrix} = \begin{Bmatrix} 0 \\ 1 \end{Bmatrix} \tag{27}$$

Hence, the torsional vibration at point D can be estimated as

$$H_{\theta_D\theta_D}(\omega) = \frac{\hat{H}_{\theta_O\theta_D}(\omega)\hat{H}_{\theta_D\theta_O}(\omega)}{\hat{H}_{\theta_O\theta_O}(\omega) - H_{\theta_O\theta_O}(\omega)} - \hat{H}_{\theta_D\theta_D}(\omega) \tag{28}$$

By utilizing Eq. (28), the effect of the additional part of the attached beam structure OD can also be removed so that the original torsional receptance of the shafting can be estimated. There is only one requirement here that the torsional vibration model of beam OD should be sufficiently accurate. It should be noticed that the process proposed in the second step can be utilized for estimation of torsional vibration receptance in cases when the shafting is modified in the form of adding or removing a shaft segment whose torsional vibration can be modelled accurately: this process can be easily extended for shafting modification, optimization and control in order to obtain required torsional vibration characteristics.

Although, in real engineering, it is highly possible that only one direct beam AOB is not enough and one additional part (beam OD) will be needed, in the following experiment, the first step to estimate the torsional receptance of structure SO is applied because step one is always

required, and only step 1 presented in section 2.3.1 is required for the specific test setup to be descried in Section 4.

3. Numerical Simulation

In order to validate the derived equations for the torsional receptance using one point translational receptance plus one cross translational receptance, a shafting system with two rigid discs is designed. The proposed method is firstly examined theoretically on the numerical model of the shafting system. As in practice the torsional receptance can be very difficult to obtain, theoretical soundness of the proposed method should be studied thoroughly at first. Then the proposed method is applied to estimate the torsional receptance of a real simple shafting structure with different setups of the attached structure using measured modal data.

3.1 Theoretical Model

Like in a real test, the receptances obtained would be contaminated by noise more or less. Therefore the effects of the parameters of the designed T-like beam structure (especially beam AOB) on the estimated torsional receptances are investigated with the numerical model. The shafting system being tested is shown in Fig. 3,

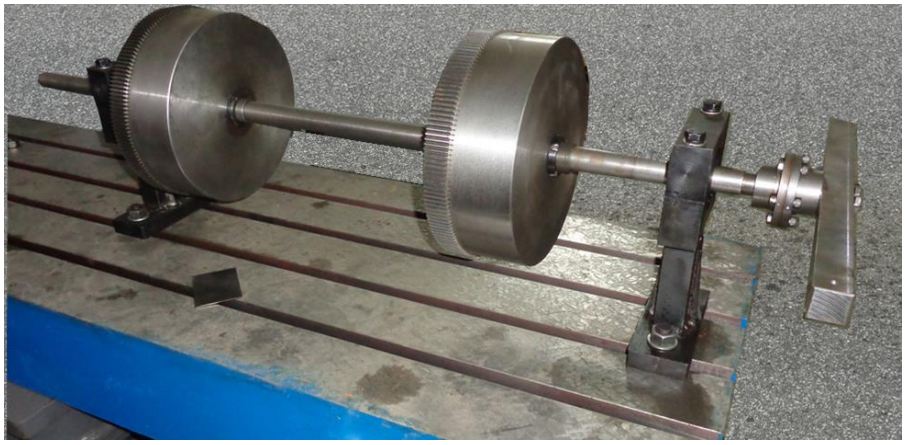

Fig. 3 Shafting system with two discs supported by two ball bearings

The related shafting parameters are as follows: l =1 m, E=2.1×10^{11} Pa, and ρ=7800 kg m^{-3}. The shafting radius r = 0.0125 m. The two identical discs are located at z = 0.3 m and z = 0.75 m approximately. The mass of the disc m =17.0 kg, the polar moment of inertia I_p = 0.210 kg m^2 and the diametric moment of inertia I_d = 0.110 kg m^2. The two bearings supporting the shaft located at z=0.2 m and z=0.9 m are assumed to be two translational springs with identical spring constants k=10^7 N/m. To clearly illustrate the locations of the discs and bearings of the assembled structure, a schematic of the FE model is also given in Fig. 4.

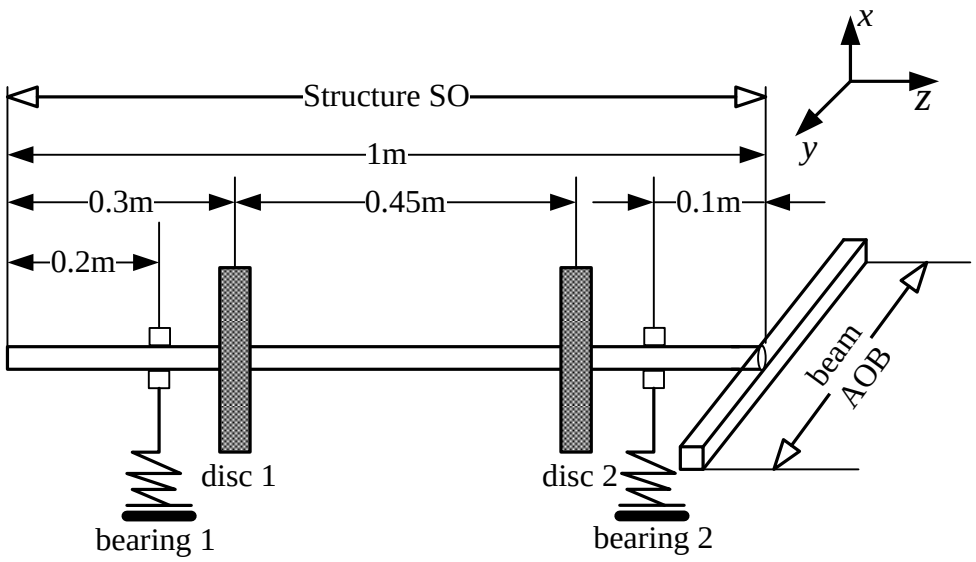

Fig. 4 Schematic of the shafting system with attached beam AOB

For the convenience of modal tests, the cross section of the attached beam AOB is designed as a square with its height being 0.025 m. The material is the same as the shafting system. Its length l_{AB} is varied in the numerical model to see if the accuracy of the estimated results is affected by it. In the FE model of structure SO, Euler-Bernoulli beam elements are used for the lateral vibration in the x-z plane (using) and torsional vibration about the z axis. In beam AOB, the same type of elements is used for the lateral vibration in the x-y plane and torsional vibration about the y axis. The length of all the elements is 0.01m. For ease of comparison, torsional receptances $H_{\theta\theta}$

obtained from the FE model of structure SO, estimated using procedure 1 and procedure 2 with 'exact' receptances H_{AA}, H_{AO} and H_{AB} obtained from the FE model, referred to as 'measured' in this section, of the whole shafting structure (SO+AOB), respectively, are plotted in Fig. 5. It can be seen that the numerical receptance directly obtained from the FE model and the estimated receptance are identical to each other in the case that no noise is included in the 'measured' data. The (first) torsional frequency is 40.8Hz.

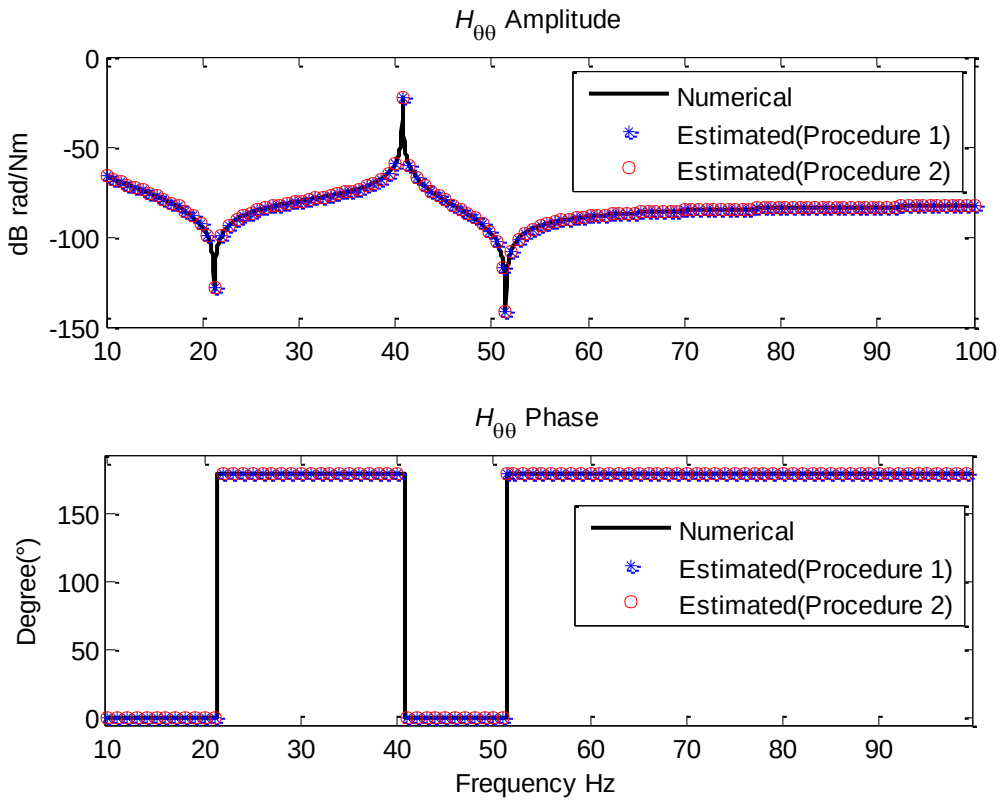

Fig. 5 Torsional Receptance of structure SO at Point O

3.2 Numerical estimation with noisy structural parameters

There is always a deviation in the nominal geometrical and material properties of a real structure/machine from their true values. The unpredictable deviations are modelled as random

variables . To assess the robustness of the current method, some structural parameters of the FE model of beam AOB are contaminated with noise and the torsional receptance is estimated.

It is assumed that every true structural parameter can be represented by one nominal value with an uncertain term. Take E for example,

$$\breve{E} = \left[1 + \alpha \times \left(2 \times RAN - 1\right)\right] \times E \tag{29}$$

where $\breve{E}$ is the uncertain Young's modulus, α is the percentage of uncertainty, RAN is a random value between 0 and 1 and E is the nominal value. In the following simulation, 100 samples are generated for $\alpha = 10\%$ for all four parameters of beam AOB: Young's modulus E, density ρ, length of beam AOB l_{AB} and height h. The 'exact' receptances H_{AA}, H_{AO} and H_{AB} are obtained from the FE model of the whole shafting structure (SO+AOB) with l_{AB} = 0.3 m and no uncertainty is included. Then with uncertainties of all the four parameters, the estimated torsional receptance with procedure 1 and procedure 2 is plotted in Fig. 6 and Fig. 7, respectively.

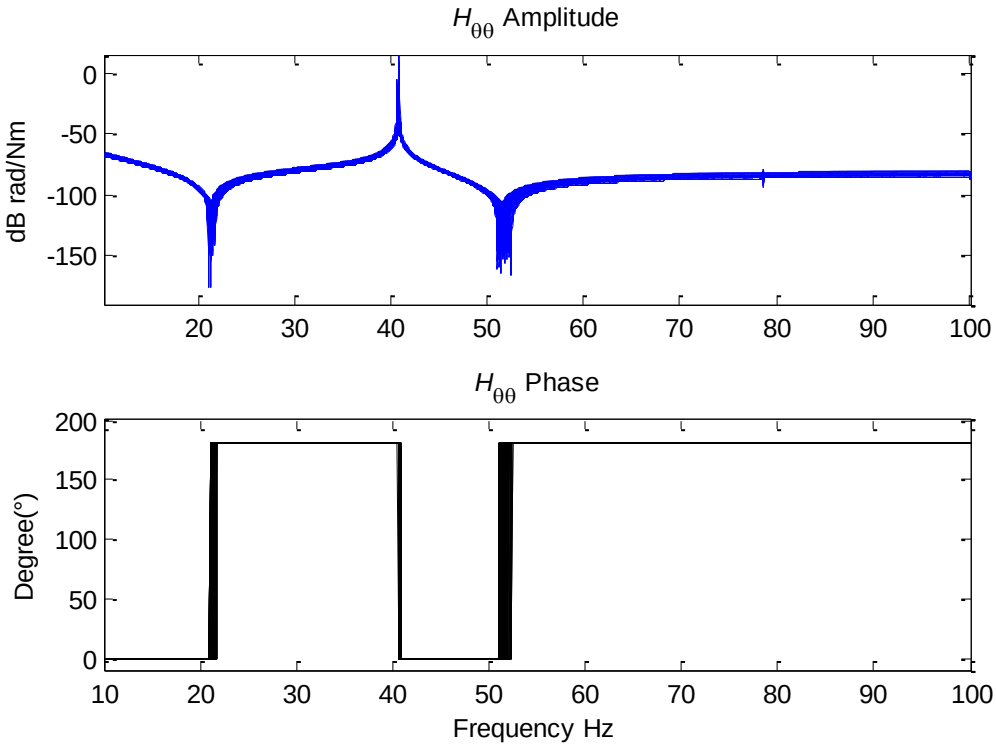

Fig. 6 Torsional Receptance at Point O (l_{AB}=0.3 m, α=10%) (Procedure 1)

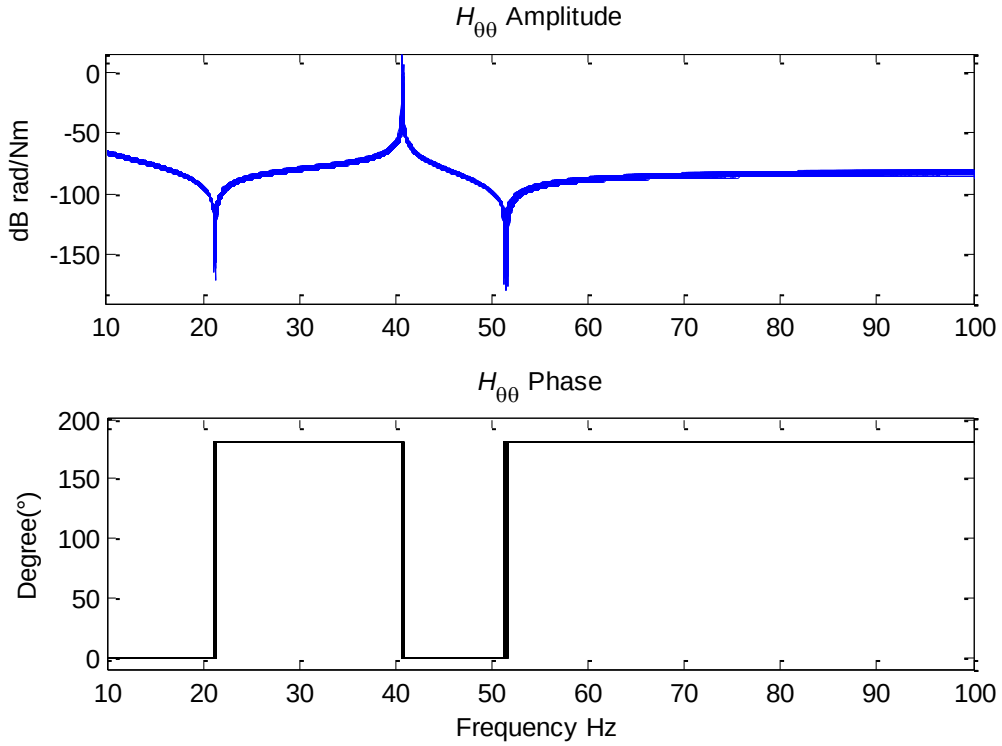

Fig. 7 Torsional Receptance at Point O (l_{AB}=0.3 m, α=10%) (Procedure 2)

A narrow scatter of the natural frequencies and zeros can be observed in Fig. 6 and Fig.7. For better comparison between procedure 1 and procedure 2, the mean and standard deviation values for the resonance and anti-resonance frequencies are given in Table 1.

Table 1 Designed, mean and standard deviation value for the resonance and anti-resonance frequencies.

	1st anti-resonance frequency	1st resonance frequency	2nd anti-resonance frequency
Designed value	21.23	40.74	51.44
mean value for procedure 1	21.26	40.75	51.5
mean value for procedure 2	21.24	40.74	51.46
standard deviation for procedure 1	0.16	0.070	0.33
standard deviation for	0.048	0.056	0.096

procedure 2

It can be seen that the proposed method is robust against parameter uncertainty of beam AOB. By comparing these two figures, the estimated results using Procedure 2 is slightly better than those estimated using Procedure 1. The uncertainties of attached beam structure AOB are shown to have a negligible effect on the final estimation results.

3.3 Numerical estimation with noisy receptance

A more general way of looking at the influence of the uncertainties in a structure is to introduce noise directly into the 'measured' receptance. Such noisy receptance data can cover a number of sources of uncertainties. One particularly interesting case is that some noisy receptance data may imply loss of symmetry of the cross section.

Theoretically, both procedure 1 and procedure 2 establish the relationship between two translational FRFs and a pure torsional FRF. However, as pointed out in [36], indirect methods would demand test data of very high quality. In real tests, due to limitation of the measurement technology, measured data always contains noise. The influences of the noise contamination are further investigated using the FE model below.

At first, point receptance (H_{AA} and H_{BB}) and cross receptance (H_{AO} in procedure 1 and H_{AB} in procedure 2) are calculated from the FE model. After this, white noise is added to the point receptances and cross receptances. To observe the effect of the noise on the estimated results, Monte Carlo simulation is made. Similar to Eq. (29), the FRFs of the assembled structure are polluted by adding random noise using the following formula:

$$\breve{A}_{me} = \left[1+\alpha\times\left(2\times RAN-1\right)\right]\times A_{me} \tag{30}$$

where $\breve{A}_{me}$ is the polluted receptance, and A_{me} is the receptance without noise. In the following simulation, 100 samples are generated for $\alpha = 10\%$ (the maximum signal-to-noise ratio is 20dB,

which occurs only when random number *RAN* is ~~identical to~~ either 0 or 1). The torsional receptance of point O is estimated for each sample. Several different lengths of the attached beam are studied. In Fig. 8 and Fig. 9, the estimated torsional receptances are plotted with the two translational FRFs both polluted with 10% noise in procedure 1 and procedure 2, respectively. In this case, the attached beam with l_{AB}=0.3 m is used. It can be seen from Fig. 8 that the estimated data, especially in the frequency range from 30Hz to 50Hz, are smooth enough. The resonant frequency of the torsional vibration of the shafting system is obtained easily and accurately, but the first anti-resonance of the shafting cannot be obtained accurately as the estimated results in the frequency range from 20Hz to 30Hz are seriously influenced by the random noise added to the translational FRFs. The second anti-resonance in the frequency range from 50Hz to 54Hz can also only be estimated approximately. Looking at Fig. 9, the results estimated using the 'measured' data at point A and point B is much better than the results estimated using the 'measured' data at point A and point O.

In order to find the possible relationship between the 'measured' translational receptances and the estimated torsional receptance under the influence of noise, point receptance H_{AA} and cross receptances H_{AO} and H_{AB} are also plotted in Fig. 10. By comparing Fig. 8 and Fig. 9, it can be found that at two peaks around 30Hz and 79Hz, the estimated torsional receptance is sensitive to noise added. It can also be observed in Fig. 10 that these two peaks are also resonant peaks for all three receptances H_{AA}, H_{AO} and H_{AB}. This phenomenon will be discussed in section 3.4 thoroughly.

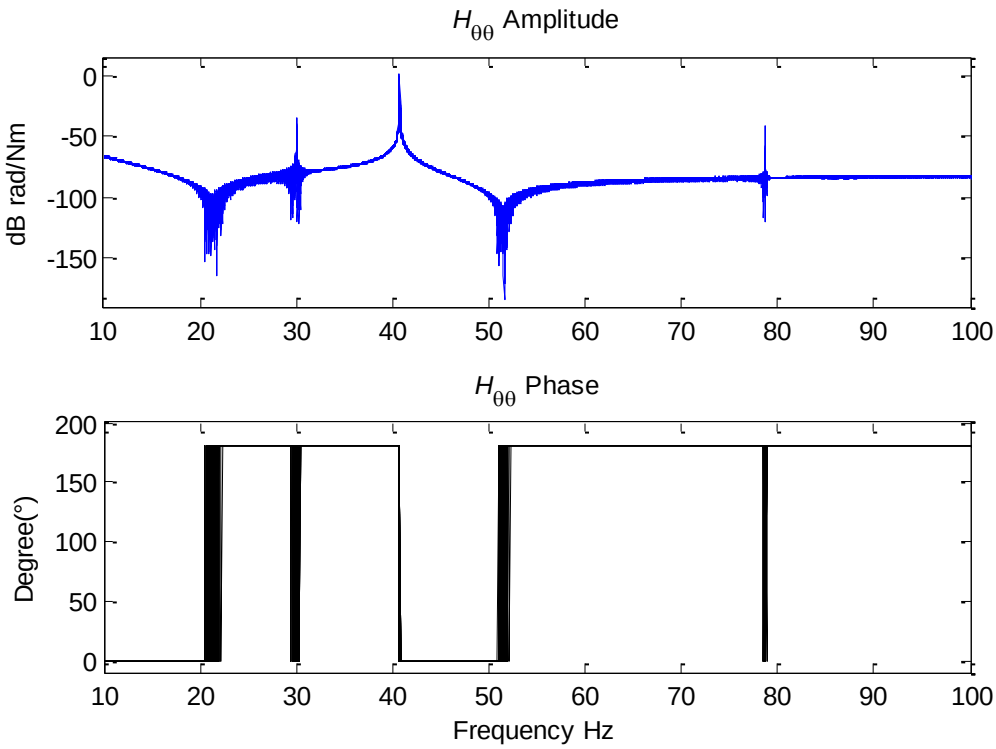

Fig. 8 Torsional Receptance at Point O (l_{AB}=0.3 m, α=10%) (Procedure 1)

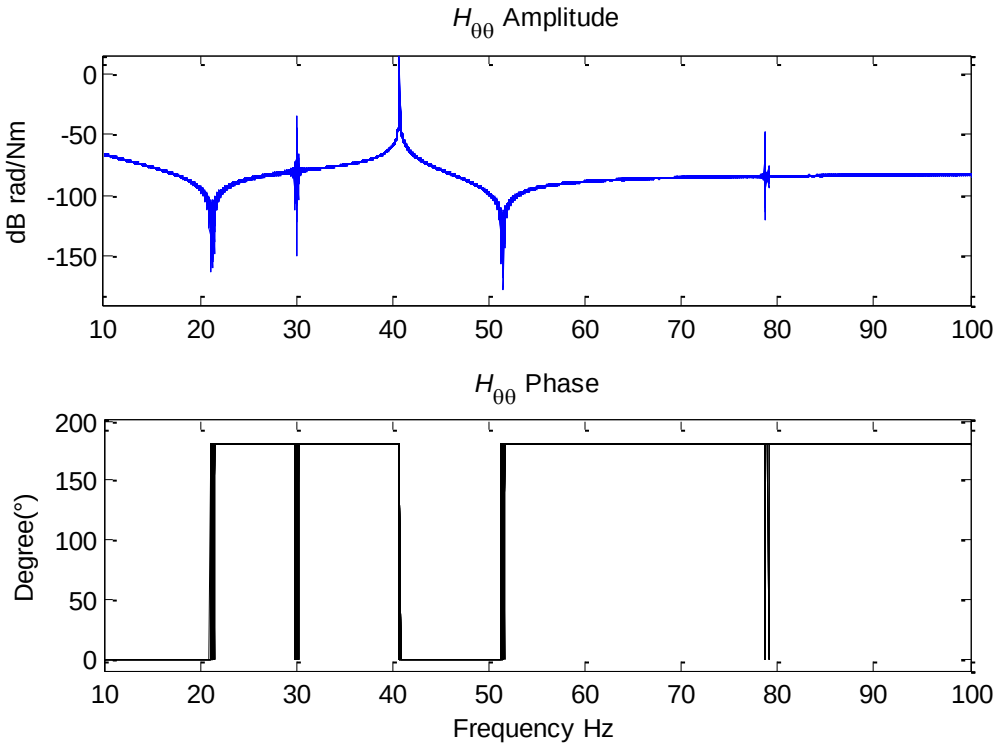

Fig. 9 Torsional Receptance at Point O (l_{AB}=0.3 m, α=10%) (Procedure 2)

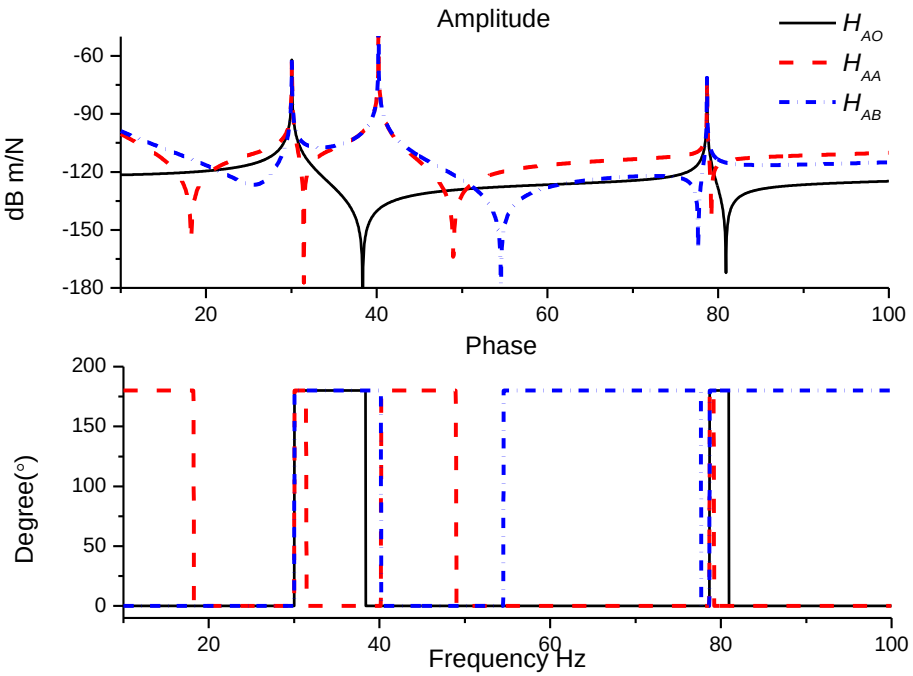

Fig. 10 Cross receptances H_{AO} and H_{AB} and point receptance H_{AA} (l_{AB}=0.3 m)

The torsional receptance and the translational receptances are also plotted with l_{AB} = 0.4 m in Fig.11-Fig.13. As can be seen from these figures obtained using procedure 1, it is possible that there exists a frequency range where the estimated results are poorer than outside this frequency range, especially when parameters of the beam such as its length are not chosen properly. From those results obtained using procedure 2, estimated result around the torsional resonant frequency and anti-resonant frequencies is slightly better compared with the estimated result obtained using procedure 1. Optimum parameters can be obtained when there exists an accurate vibration model of the original shafting system. However, in most cases in engineering, the shafting cannot be modelled accurately; In real tests, T-blocks of different characteristics can be used and several tests should be done.

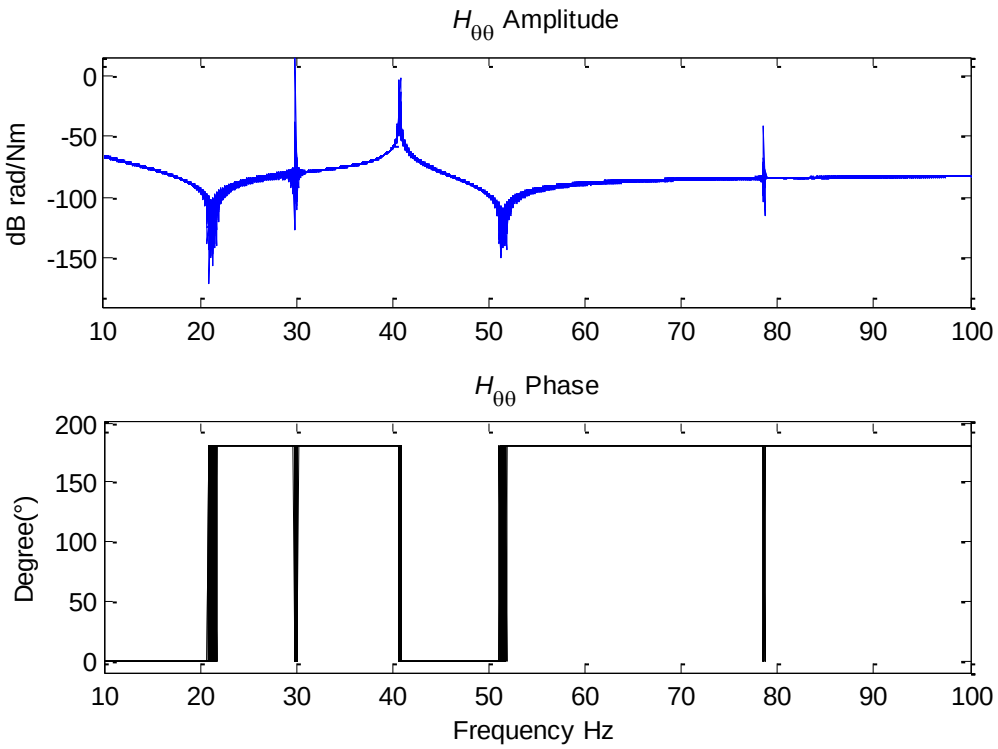

Fig. 11 Torsional Receptance at Point O (l_{AB}=0.4 m, α=10%) (Procedure 1)

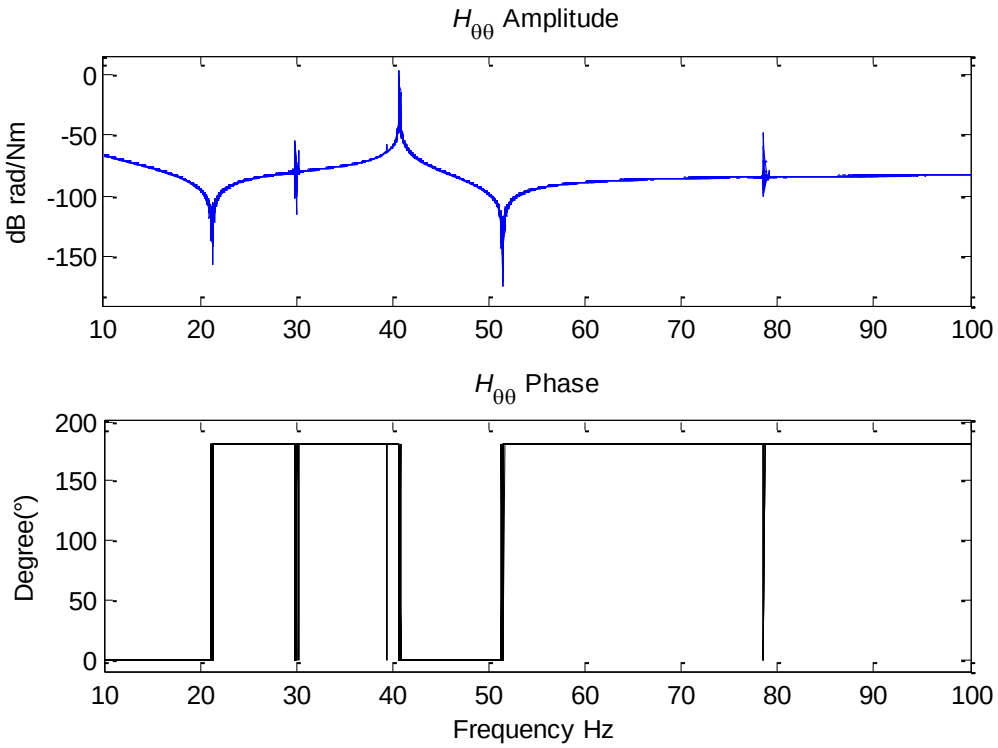

Fig. 12 Torsional Receptance at Point O (l_{AB}=0.4 m, α=10%) (Procedure 2)

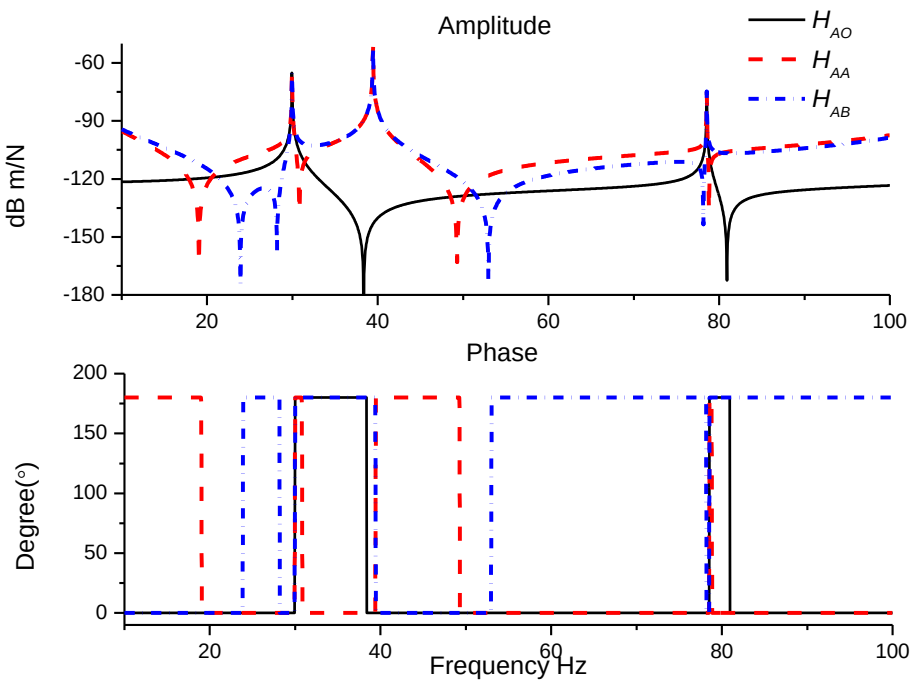

Fig. 13 Cross receptances H_{AO} and H_{AB} and point receptance H_{AA} (l_{AB}=0.4 m)

3.4 Appearance of bending Frequencies in Torsional Receptance

An interesting phenomenon can be recognised by comparing Fig. 5 with torsional receptance graphs such as Figs. 8 and 9. It can be observed that there are two extra peaks at 30Hz and 79Hz in the torsional receptance curves when noise is introduced into the 'measured' cross and point translational receptances of point A, O and B.

It turns out that these two additional peaks are the first and third bending frequencies of the shafting system. It may seem odd that a torsional receptance would involve bending frequencies. A second thought should remove this doubt. When noise is introduced into structural parameters in Section 3.2, for example, in *E*, the whole structure remains symmetric. For procedure 2, measured data at points A and B which are symmetrical to point O is used. As a result, a pure torque applied at point O will only excite torsional vibration around the *z* axis and therefore only

the first torsional frequency is present in the torsional receptance in the frequency range under investigation (see Fig. 7 for example).

On the other hand, when noise is directly introduced into 'measured' cross and point translational receptances of point A, O and B, the symmetry of the structure is violated for some samples. As a result, a pure torque applied at point O excites not only torsional vibration about the *z* axis but also bending vibration in the *x* direction, and therefore contributions from bending vibration will be present in the torsional receptance in this particular shafting system, in the form of two additional peaks of the bending frequencies. This is a new and interesting issue that was not encountered in [38] and [40] when rotational receptances were estimated.

The reason why the second bending frequency is not observed can be explained by vibration characteristics of complete shafting structure (SO+AOB). Here, the first three bending mode shapes of the complete shafting structure with l_{AB}=0.3 m are plotted in Fig. 14. It can be seen in Fig. 14 that the first and third bending modes that appear on beam AOB are both symmetrical about point O; however, the second bending mode is asymmetrical about point O and it has no *x*-displacement at point O. Additionally, an excitation in the *x* direction at any point along AOB can be thought of as the same force in the *x* direction acting at point O and a torque acting about point O whose amount is the force multiplied by the distance between this point and point O. The former (the same force in the *x* direction acting at point O) does not excite the second bending mode because point O is a node of the second mode.

1st order mode shape of the assembled structure (f=30.04Hz)

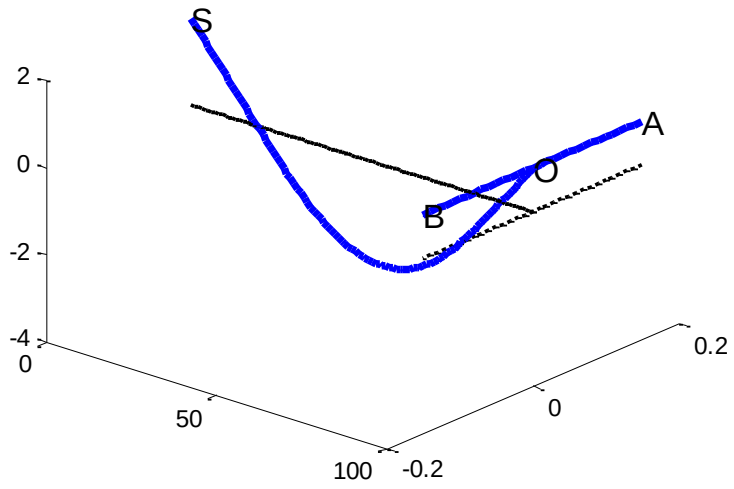

(a)

2nd order mode shape of the assembled structure (f=40.20Hz)

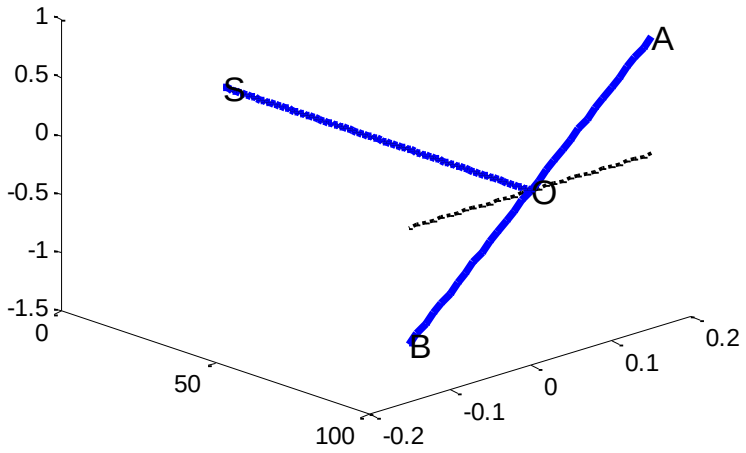

(b)

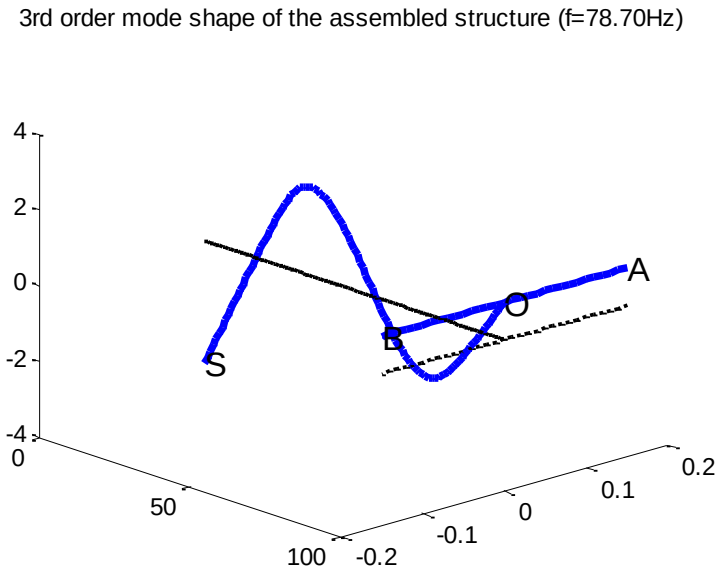

(c)

Fig. 14 First three mode shapes of the assembled structure (the dark line denotes the original position). The first (a), second (b) and third (c) mode shapes.

In some cases, it is desired to identify the torsional vibration frequencies among all frequencies. One possible way to identify different kinds of frequencies is observing the peaks of measured translational receptance in relation to the peaks of the estimated torsional receptance. A peak frequency f_k is very likely to be a coupled frequency (a bending frequency appearing in the torsional receptance), if it is also the resonant peak of all measured cross receptances H_{AO} and H_{AB} and point receptance H_{AA}.

It is not easy to identify such coupled frequencies where there is noise contamination in measured data as torsional vibration is coupled with bending vibration. Since the supports (for example, bearings) to a shafting systems have a negligible influence on torsional vibration but a significant influence on bending vibration of the shafting, one way to identify which peaks in the torsional receptance are coupled frequencies is to repeat the estimation procedure described above on the same shafting system with changed support positions. Any peaks that undergo a

noticeable change in location in the estimated new torsional receptance must be due to bending and thus are coupled ones.

In order to check this, the first bearing is moved from z= 0.2 m to 0.1 m, and then the translational receptances are 'measured' again and the new estimated torsional receptance is estimated. These are also plotted in Figs. 15-16. In Fig. 15, the first resonant frequency now shifts approximately from 30Hz to 23Hz and the third one from 79Hz to around 63 Hz, while the second one remains unchanged in its location (value). In real applications, a modification can usually be made to the supporting system of the shafting to preserve the torsional vibration characteristics but change other vibration characteristics, or the other way around. This process to identify the coupled frequency is more reliable compared with the process of observing all measured cross receptances H_{AO} and H_{AB} and point receptance H_{AA} only, although this may cost a little more, especially in real engineering applications.

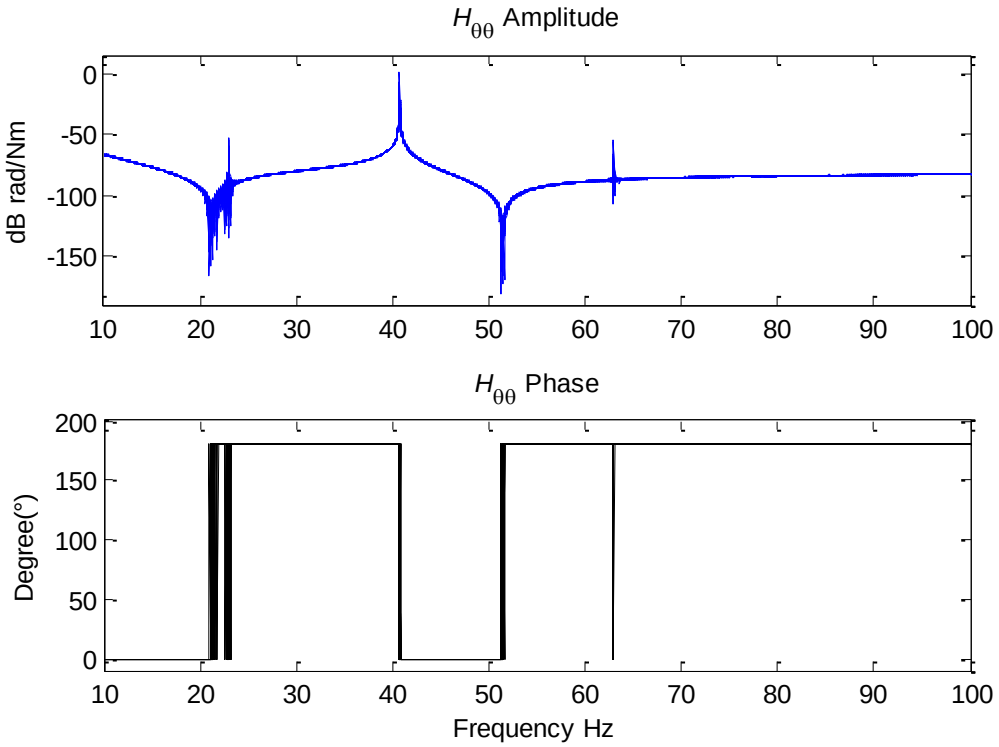

Fig. 15 Torsional Receptance at Point O (l_{AB}=0.4 m, α=10%) (Procedure 2) (with the position of the first spring shifted)

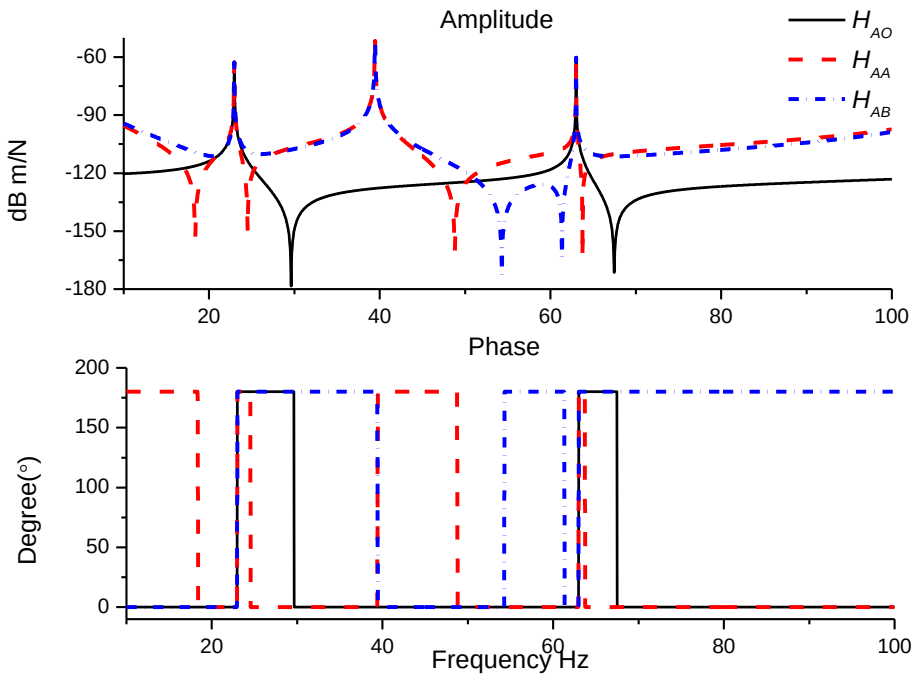

Fig. 16 Cross receptances H_{AO} and H_{AB} and point receptance H_{AA} (l_{AB}=0.4 m) (with the position of the first spring shifted)

4. Experimental Validation

To verify the proposed method, translational FRFs of a real shafting system shown in Fig. 3 are measured and estimated torsional receptance is obtained. As for attached structure (beam AOB), it is a very simple structure which can be modelled easily and accurately, only the Young's modulus is updated from E=2.1×10^{11} to E=1.96×10^{11} with one simple modal test. Considering the main concern of this paper, details of this modal test and the updating process are not given here. As exact torsional receptance for the shafting system cannot be obtained directly, estimated results with different lengths of the attached beam are analysed and compared. In the experiment, three DeltaTron Accelerometers of type 4526 from Brüel & Kjær are used

with measurable amplitude in frequency range from 0.3 Hz to 8 kHz and measurable phase in frequency range from 2 Hz to 5 kHz for phase. An impact hammer of type 8206-003 from Brüel & Kjær is used. As the concerned frequency range is below 100Hz, a rubber tip is used. For this experiment, there exist two small holes in the centre of beam AOB so that it can be attached to the shafting system via a small coupling firmly with two screws.

For comparison, both estimation results with procedure 1 and procedure 2 are given. Firstly, the experimental cross receptances H_{AO} and H_{AB} and point receptance H_{AA} are plotted in Fig. 17 with l_{AB} = 0.3m. The estimated results of torsional receptance using procedure 1 are shown in Fig. 18. As in procedure 2, cross receptance H_{AO} can also be estimated using translational receptances H_{AB} and H_{AA}. In order to verify the correctness of procedure 2, both the measured cross receptance $H_{AO}^{\mathrm{measured}}$ and the estimated cross receptance $H_{AO}^{\mathrm{estimated}}$ are given firstly in Fig.19. It can be seen that procedure 2 can estimate cross receptance H_{AO} accurately. Then, in Fig. 20, the torsional vibration receptance estimated using procedure 2 is presented.

It can be seen from Fig. 18, especially for the phase in the range from 20Hz to 30Hz, that the estimated results are not quite accurate and are sensitive to noise in the measured data. One reason is the limitations of the test equipment: the measured data contains more noise in lower frequency range. As discussed in section 3.4, in case when a frequency f_k is the resonant peak for all cross receptances H_{AO} and H_{AB} and point receptance H_{AA}, it is highly likely to be a coupled frequency. As the axial symmetry of shafting structure SO is not guaranteed, coupled bending and torsional vibration then occurs which affects the final torsional receptance estimation. By comparing Fig. 20 and Fig. 18, the estimated torsional receptance between 20Hz and 30Hz becomes much better in Fig. 20. However, around 70Hz in this figure, one small peak appears which is not obvious in Fig. 18. Turning back to Fig. 17 again, it could also be found very clearly

that this is a resonant peak for all cross receptances H_{AO} and H_{AB} and point receptance H_{AA}. This small peak in torsional receptance is also caused by the coupling of torsional and bending vibration.

Similaly, both measured data and estimated results with l_{AB} = 0.4 m are shown in Figs. 21-24. Similar phenomena can be found in these four figures like Figs. 17-20. By comparing Fig. 19 and Fig. 23, especially the phase plot, the cross receptance H_{AO} estimated with l_{AB} = 0.4 m is slightly better. In Fig. 24, it can be seen that both the amplitude and phase become smoother around 70Hz. In such a case, the peak around 70Hz in Fig. 20 and Fig. 22 should be considered a coupled frequency and is not the resonant peak of pure torsional receptance.

By comparing all these estimated results in Figs. 18, 20, 22 and 24, the first natural frequency is all approximately equal to 42.75Hz. The second anti-resonant frequency is equal to 51Hz. As for the first anti-resonant frequency, the estimated results look fuzzy from the results obtained using procedure 1 in both Fig. 18 and Fig. 22. The first anti-resonant peak can be obtained from Fig. 20 (around 22 Hz) or from Fig. 24 (around 20.25 Hz) for. Although they are still different, the estimated receptance is much better compared with the results obtained using procedure 1.

There are several reasons why all these estimated results of amplitude and phase are not identical to one another, especially in the range from 20Hz to 30Hz for Figs. 18, 20, 22 and 24. One reason is the error contained in the measured data. Another is the modelling errors of beam AOB — the difference between the finite element model and the real structure. As for the example presented here, one beam structure AOB is directly connected to the shafting system via one coupling and hence step two to estimate the torsional receptance of point D from that of point O, presented in section 2, is not needed here. In the cases when beam OD is included, the accuracy of the torsional vibration model of beam OD would also affect the final estimation. A

third important possibility which should also be taken into account is how the T-like beam structure is attached to the shafting system: the connection is of vital importance for the proposed method, as if it cannot connect firmly or be positioned to the centre point of the shafting, the poor connection would then affect the final estimated torsional receptance. The connector between the attached T-block and the original shafting system should also be considered in the FE model of the T-block to enhance the accuracy of the estimated torsional receptance if it is suspected that it is not rigid enough.

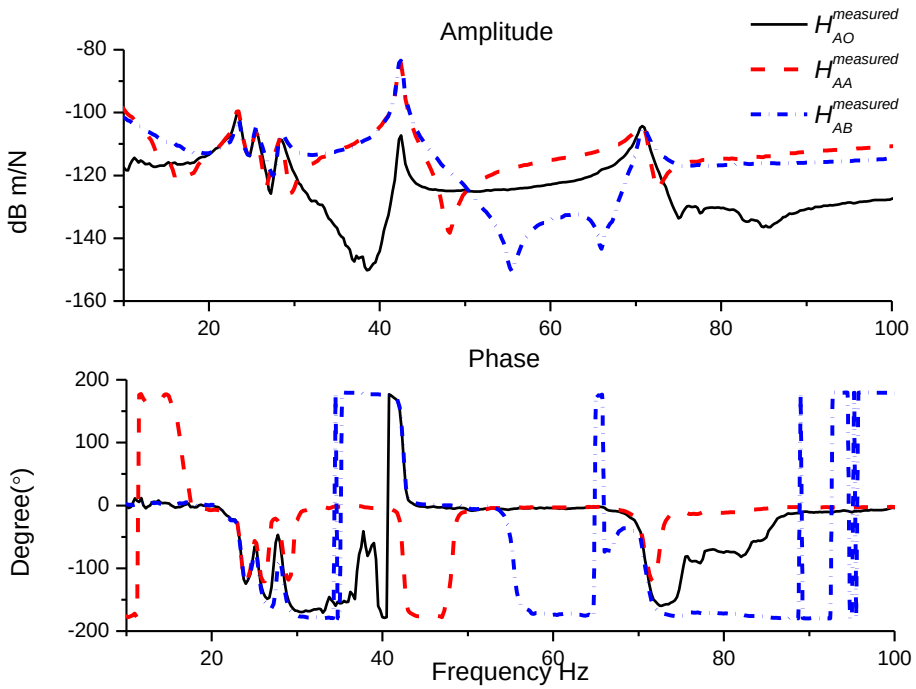

Fig. 17 Measured cross receptances H_{AO}^{measured} and H_{AB}^{measured} and point receptance H_{AA}^{measured} (l_{AB}=0.3 m)

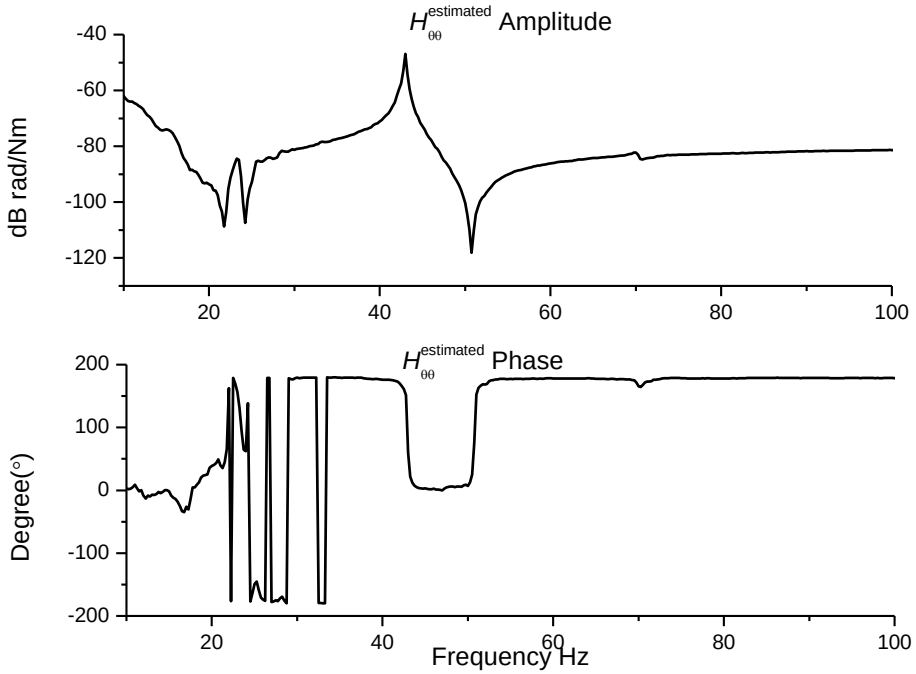

Fig. 18 Torsional receptance at point O (l_{AB}=0.3 m) (Procedure 1)

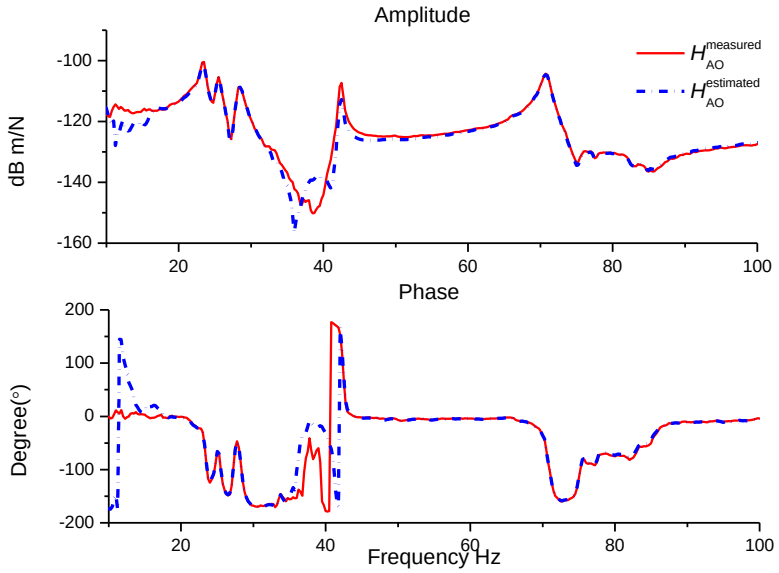

Fig. 19 Estimated cross receptance $H_{AO}^{estimated}$ and measured cross receptance $H_{AO}^{measured}$ (l_{AB}=0.3 m)

(Procedure 2)

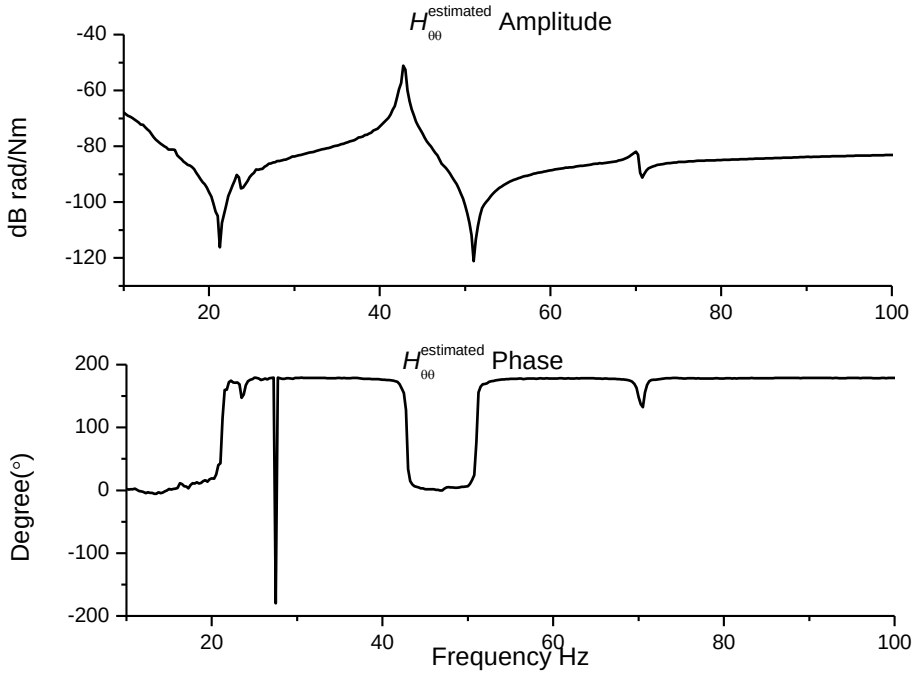

Fig. 20 Torsional receptance at point O (l_{AB}=0.3 m) (Procedure 2)

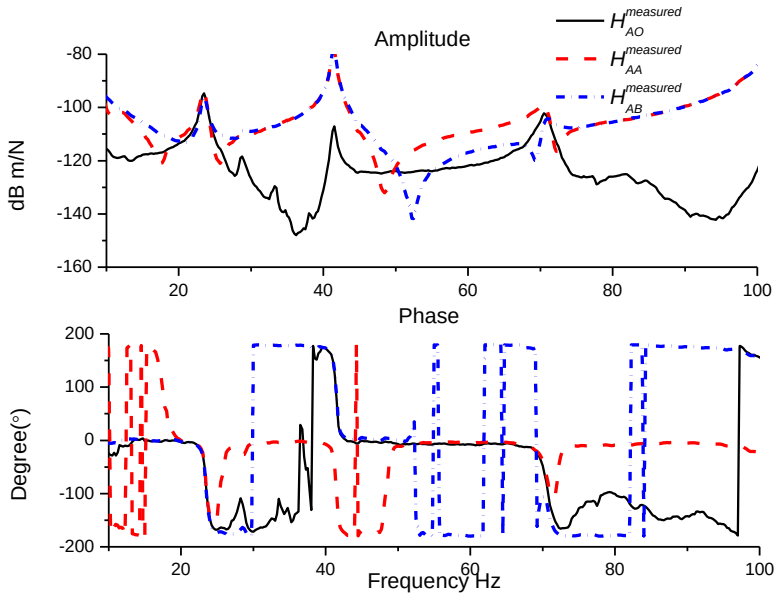

Fig. 21 Measured cross receptances $H_{AO}^{measured}$ and $H_{AB}^{measured}$ and point receptance $H_{AA}^{measured}$ (l_{AB}=0.4 m)

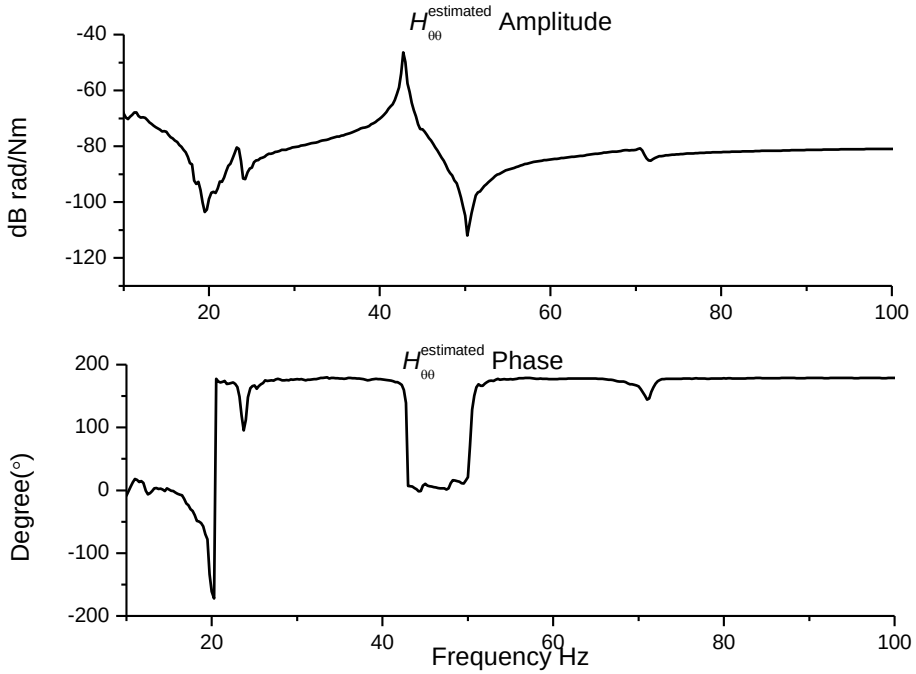

Fig. 22 Torsional receptance at point O (l_{AB}=0.4 m) (Procedure 1)

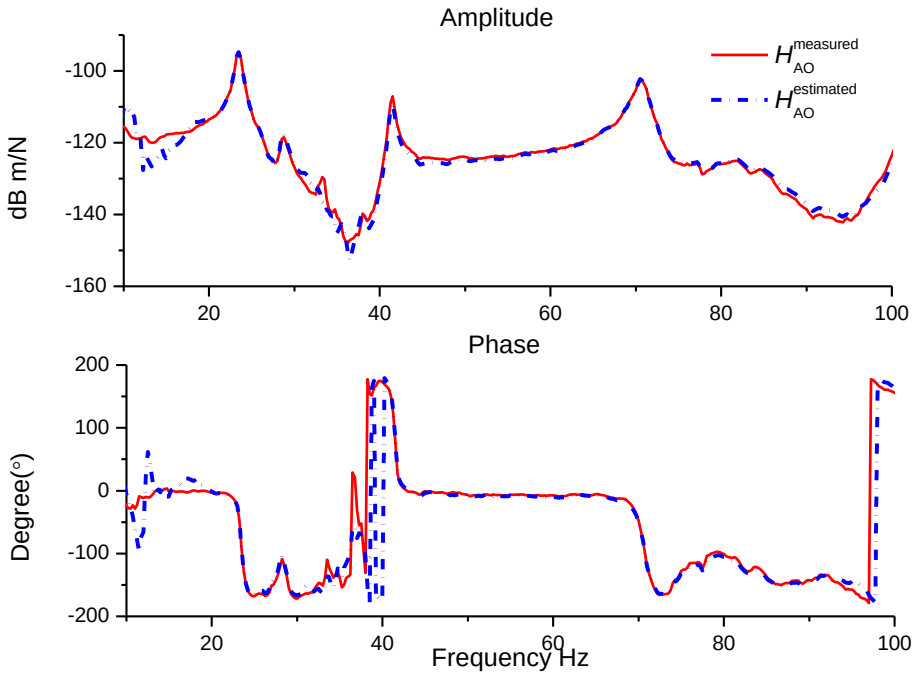

Fig. 23 Estimated cross receptance $H_{AO}^{\text{estimated}}$ and measured cross receptance H_{AO}^{measured} (l_{AB}=0.4 m)

(Procedure 2)

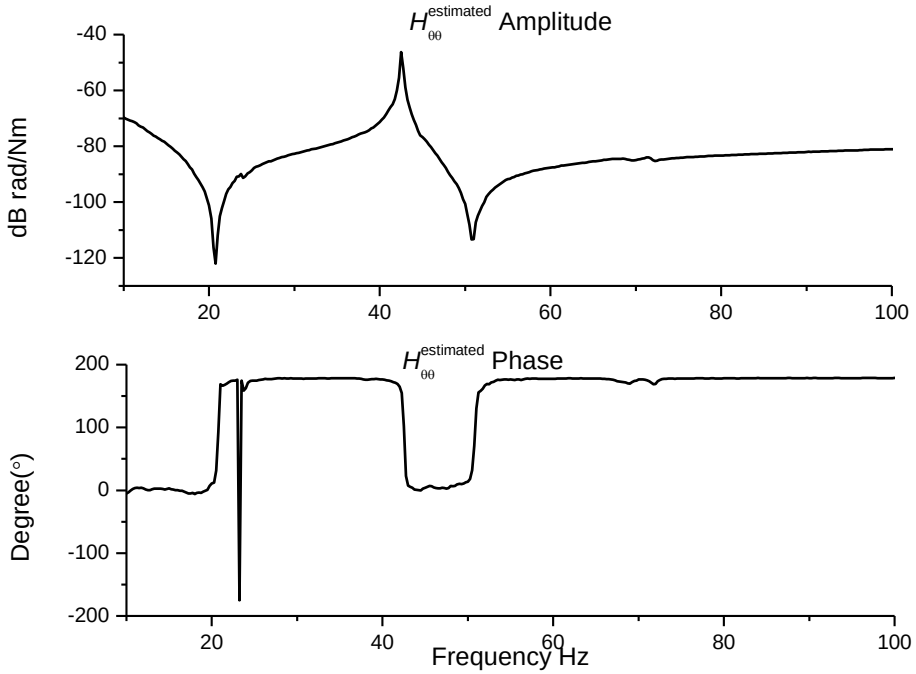

Fig. 24 Torsional receptance at point O (l_{AB}=0.4 m) (Procedure 2)

5. Conclusions

In this paper, one indirect method is presented for estimating torsional receptance of shafting systems from measured translational receptance data. One beam or T-like beam structure is attached to the shafting system and the relationship between the torsional receptance of the shafting and the translational receptance of the assembled structure are established. Two different procedures are presented. Several aspects which affect the measurement accuracy are discussed, considering vibration tests would always contain measurement noise and real shafting systems always have uncertainty in geometric/material properties. The numerical part of the method is shown to be sufficiently accurate and robust even when the parameters of the attached beam structure and the receptance data of the numerical model are contaminated with as high as 10% noise. Estimation results from simulated examples of attached beams of different lengths are analysed. The appearance of bending frequency in the torsional resonance is studied both

theoretically and experimentally in detail. Two reliable procedures are also given to identify such bending frequencies in the estimated torsional receptance. The second procedure of modifying the shaft to shaft bending frequencies while keeping the torsional ones unchanged seems a more slightly expensive but reliable method.

Modal test data of a shafting directly attached with a straight beam is used to reveal the torsional receptance of the shafting structure at one end point. It can be seen from the experimental results that the proposed method can be used to estimate the torsional receptance with enough accuracy, which can be used to update FE models, conduct structural identification and diagnosis, make structural modifications or carry out vibration control of real rotating machineries.

Acknowledgements

The authors gratefully acknowledge the financial support from National Natural Science Foundation of China (Grant No. 51375104). The main part of the theoretical work was carried out at the School of Engineering, University of Liverpool, during the year-long visit by the first author under the supervision of the second author.

REFERENCES

[1] M.I. Friswell, J.E.T. Penny, S.D. Garvey, A.W. Lees, Dynamics of rotating machines, Cambridge University Press, Cambridge ; New York, 2010.
[2] N.A. Halliwell, The laser torsional vibrometer: A step forward in rotating machinery diagnostics, Journal of Sound and Vibration, 190 (1996) 399-418.
[3] G. Genta, Dynamics of rotating systems, Springer, New York, 2005.
[4] D.J. Ewins, Modal testing: theory, practice, and application, 2nd ed., Research Studies Press, Baldock, Hertfordshire, England ; Philadelphia, PA, 2000.
[5] D.N. Walker, Torsional vibration of turbomachinery, McGraw-Hill, Inc, NewYork, 2004.
[6] H. Luo, R. Chumai, N. Peton, B. Howard, A. Menon, Torsional vibration Detection Using High Sampling Rate and High Resolution Keyphasor Information, in: Proceedings of the ASME 2013 International Design Engineering Technical Conference and Computers and Information in Engineering Conference, ASME, Oregon, USA, 2013.
[7] J. Tůma, L. Smutný, P. Kočí, Experiences and Device of R&D Laboratory of Noise and Vibration Diagnostics at Department of Control Systems & Instrumentation VŠBTU Ostrava, Principia Cybernetica, 3 (2003) 148-152.
[8] T.J. Miles, M. Lucas, N.A. Halliwell, S.J. Rothberg, Torsional and bending vibration measurement on rotors using laser technology, Journal of Sound and Vibration, 226 (1999) 441-467.
[9] M.L.M. Duarte, D.J. Ewins, Rotational degrees of freedom for structural coupling analysis via finite-difference technique with residual compensation, Mechanical Systems and Signal Processing, 14 (2000) 205-227.
[10] C. Sihler, A novel torsional exciter for modal vibration testing of large rotating machinery, Mechanical Systems and Signal Processing, 20 (2006) 1725-1740.
[11] H. Kim, C.I. Park, S.H. Lee, Y.Y. Kim, Non-contact modal testing by the electromagnetic acoustic principle: Applications to bending and torsional vibrations of metallic pipes, Journal of Sound and Vibration, 332 (2013) 740-751.
[12] M.I. Friswell, J.E. Mottershead, Finite element model updating in structural dynamics, Kluwer Academic Publishers, Dordrecht ; Boston, 1995.
[13] Z. Feng, M.J. Zuo, F. Chu, Application of regularization dimension to gear damage assessment, Mechanical Systems and Signal Processing, 24 (2010) 1081-1098.
[14] Y. Lin, F. Chu, The dynamic behavior of a rotor system with a slant crack on the shaft, Mechanical Systems and Signal Processing, 24 (2010) 522-545.
[15] J.-J. Sinou, On the use of non-linear vibrations and the anti-resonances of higher-order frequency response functions for crack detection in pipeline beam, Mech Res Commun, 43 (2012) 87-95.
[16] J.-J. Sinou, Effects of a crack on the stability of a non-linear rotor system, Int J Nonlin Mech, 42 (2007) 959-972.
[17] E.H. Maslen, C.K. Sortore, J.A. Vázquez, C.R. Knospe, Synchronous response estimation in rotating machinery, Journal of Engineering for Gas Turbines and Power, 124 (2002) 357-362.
[18] R. Ricci, P. Pennacchi, E. Pesatori, G. Turozzi, Modeling and Model Updating of Torsional Behavior of an Industrial Steam Turbo Generator, Journal of Engineering for Gas Turbines and Power, 132 (2010).
[19] P. Pennacchi, N. Bachschmid, A. Vania, G.A. Zanetta, L. Gregori, Use of modal representation for the supporting structure in model-based fault identification of large rotating

machinery: Part 1—theoretical remarks, Mechanical Systems and Signal Processing, 20 (2006) 662-681.
[20] P. Pennacchi, N. Bachschmid, A. Vania, G.A. Zanetta, L. Gregori, Use of modal representation for the supporting structure in model-based fault identification of large rotating machinery: Part 2—application to a real machine, Mechanical Systems and Signal Processing, 20 (2006) 682-701.
[21] J.E. Mottershead, Y.M. Ram, Inverse eigenvalue problems in vibration absorption: Passive modification and active control, Mechanical Systems and Signal Processing, 20 (2006) 5-44.
[22] H. Nevzat Özgüven, Structural modifications using frequency response functions, Mechanical Systems and Signal Processing, 4 (1990) 53-63.
[23] J.E. Mottershead, C. Mares, M.I. Friswell, An inverse method for the assignment of vibration nodes, Mechanical Systems and Signal Processing, 15 (2001) 87-100.
[24] A. Kyprianou, J.E. Mottershead, H. Ouyang, Assignment of natural frequencies by an added mass and one or more springs, Mechanical Systems and Signal Processing, 18 (2004) 263-289.
[25] H. Ouyang, D. Richiedei, A. Trevisani, G. Zanardo, Eigenstructure assignment in undamped vibrating systems: A convex-constrained modification method based on receptances, Mechanical Systems and Signal Processing, 27 (2012) 397-409.
[26] B. Dobson, E. Rider, A review of the indirect calculation of excitation forces from measured structural response data, Proceedings of the Institution of Mechanical Engineers, Part C: Journal of Mechanical Engineering Science, 204 (1990) 69-75.
[27] P. Pennacchi, Robust estimation of excitations in mechanical systems using M-estimators—Experimental applications, Journal of Sound and Vibration, 319 (2009) 140-162.
[28] P. Pennacchi, Robust estimate of excitations in mechanical systems using M-estimators—Theoretical background and numerical applications, Journal of Sound and Vibration, 310 (2008) 923-946.
[29] Z. Li, Z. Feng, F. Chu, A load identification method based on wavelet multi-resolution analysis, Journal of Sound and Vibration, 333 (2014) 381-391.
[30] P. Avitabile, J. O'Callahan, Frequency response function expansion for unmeasured translation and rotation Dofs for impedance modelling applications, Mechanical Systems and Signal Processing, 17 (2003) 723-745.
[31] S.H. Yap, B.M. Gibbs, Structure-borne sound transmission from machines in buildings, part 2: Indirect measurement of force and moment at the machine-receiver interface of a single point connected system by a reciprocal method, Journal of Sound and Vibration, 222 (1999) 99-113.
[32] S.H. Yap, B.M. Gibbs, Structure-borne sound transmission from machines in buildings, part 1: Indirect measurement of force at the machine-receiver interface of a single and multi-point connected system by a reciprocal method, Journal of Sound and Vibration, 222 (1999) 85-98.
[33] M.A. Sanderson, C.R. Fredö, Direct measurement of moment mobility: part I: A theoretical study, Journal of Sound and Vibration, 179 (1995) 669-684.
[34] M.A. Sanderson Direct measurement of moment mobility: part II: An experimental study, Journal of Sound and Vibration, 179 (1995) 685-696.
[35] J. Su, B.M. Gibbs, Measurement of point moment mobility in the presence of non-zero cross mobility, Applied Acoustics, 54 (1998) 9-26.
[36] J. Silva, N. Maia, A. Ribeiro, Indirect estimation of rotational frequency-response-functions, in: Proc of the 19th International Modal Analysis Conference. Orlando: IMAC, 2001.

[37] J. Dong, K.G. McConnell, Extracting multi-directional FRF matrices with ‘‘Instrument Cluster’’, in: Proceedings of the 20th International Modal Analysis Conference (IMAC XX), 2002, pp. 751-764.
[38] J.E. Mottershead, A. Kyprianou, H. Ouyang, Structural modification. part 1: Rotational receptances, Journal of Sound and Vibration, 284 (2005) 249-265.
[39] A. Kyprianou, J.E. Mottershead, H. Ouyang, Structural modification. part 2: Assignment of natural frequencies and antiresonances by an added beam, Journal of Sound and Vibration, 284 (2005) 267-281.
[40] J.E. Mottershead, M.G. Tehram, D. Stancioiu, S. James, H. Shahverdi, Structural modification of a helicopter tailcone, Journal of Sound and Vibration, 298 (2006) 366-384.